FACULTY OF TECHNOLOGY

ALTERNATIVE ALKALI ACTIVATOR FOR BLAST FURNACE SLAG AND STONE WOOL

Amarachi Blessing Ezu

ENVIRONMENTAL ENGINEERING
Master's thesis
November 2019

THESIS ABSTRACT

University of Oulu Faculty of Technology

Degree Programme (Master's Thesis)	Major Subject (Licentiate Thesis)
Master's Degree Programme (BCBU) in Environmental Engineering	Clean production, Energy and Environmental Engineering
Author	**Thesis Supervisor**
Ezu Amarachi Blessing	Adesanya Damilola Elijah (M.Sc.), Dr. Katja Ohenoja, Dr. Päivö Kinnunen

Title of Thesis

Alternative Alkali Activator for Blast Furnace Slag and Stone wool

Major Subject	Type of Thesis	Submission Date	Number of Pages
Clean Production	Master's Thesis	November, 2019	89

Abstract

The utilization of desulphurization dust from the steel production as an alternative alkali activator for stone wool (SW) and blast furnace slag (BFS) was investigated in this thesis. These materials are industrial by-products considered as an alternative construction material for mitigating CO_2 emissions associated with cementing materials, and to reduce their landfilling.

Previous literatures on alkali activated geopolymers were reviewed to establish the concept of utilizing industrial wastes or by-products in producing eco-friendly and sustainable alkali activated cementing materials equivalent to standard cementitious materials. The experimental procedure used in this study was the "one-part mix pathway" to achieve adequate paste workability and the highest mechanical strength via the various mix compositions which includes; constant water/binder (w/b) ratio, and varying ratios of silicon, calcium and sodium oxides. Also, addition of different percentages (0%, 0.05%, 0.10% and 0.15%) of Triisopropanolamine (TIPA) was used to aid in the dissolution of minerals. The amount of the desulphurization dust was kept constant in all mix compositions.

The different mix composition contained various percentages (0%, 5%, 10%, and 15%) of stone wool and were cured at 60 ºC for 24 hours. Mechanical strength was tested at 7-day and 28-day. The highest compressive strength of 20.1 MPa was recorded at 28-day when 0.05% TIPA was added to 5% SW samples. A very good workability (96.2%) was observed when 0.1% TIPA was added to 5% SW samples.

In addition, characterization of the alkali activated geopolymer pastes was carried out using XRD, TGA and iso-thermal microscopy techniques to analyze the reaction products.

Overall result showed that desulphurization dust can effectively activate geopolymer precursors to produce desirable mortars, while SW is an appropriate co-binder to blast furnace slag, with an optimum amount observed to be 5% stone wool. Also, the effect of TIPA was significant in the workability and mechanical strength of the paste.

Keywords: Desulphurisation dust, Stone wool, Blast furnace slag, Triisopropanolamine (TIPA)

Forward

The purpose of this thesis was to examine the possibility of using de-sulphurization dust as an alternative alkali activator for blast furnace slag and stonewool, to produce a sustainable geopolymer mortar. This research work was done at the fibre and particle engineering laboratory, University of Oulu, under the SYMMET project.

I am grateful to God for enabling me to achieve this success. I appreciate the leadership of fibre and particle research unit chaired by Prof. Mirja Illikainen and especially Dr Katja Ohenoja and Dr. Zahra Abdollahnejad for their assistance towards ensuring my internship and master's thesis with the group, and Dr Paivo Kinnunen for his significant input in this thesis. Many thanks to Adesanya Damilola Elijah for supervising and guiding me all through the research period. I am thankful to Elisa for her care and support at the laboratory.

My sincere gratitude goes to my husband, Shedrack Ezu, for his immense support, love and prayers, to my lovely kids (Olivia, Stephanie and Sophia) for keeping me active, to my sister, Ebere, for her care and support, and to my friend Chibuzor, for her motivational encouragements.

Oulu, 12.11.2019 Ezu Amarachi Blessing

TABLE OF CONTENTS

SYMBOLS AND ABBREVIATIONS

σF	Flexural strength
σc	Compressive strength
ASTM	American society for testing and materials
CDW	Construction and demolition waste
BFS	Blast furnace slag
DE-DUST	Desulphurization dust
RHA	Rice husk ash
FAETP	Fresh water aquatic ecotoxicity potential
LCA	Life cycle assessment
SCM	Supplementary cementitious material
GHG	Greenhouse gas
SW	Stone wool
GW	Glass wool
RW	Rockwool
AASC	Alkali activated slag concrete
C-A-S-H	Calcium alumino silicate hydrate
C-S-H	Calcium silicate hydrate
NASH	Sodium alumino silicate hydrate
MAETP	Marine aquatic ecotoxicity potential
HTP	Human toxicity potential
GWP	Global warming potential
MPa	Mega Pascal
Mt.	Metric ton
wt. %	Weight in percentage

1. Introduction

1.1 Background

The use of raw materials in a sustainable manner is trending for future advancement, especially with increment in the human population. A significant amount of natural resources is consumed when producing building and construction materials. For example, in the production of 1 tonne of ordinary Portland cement (OPC), amount of raw materials needed is up to 1.7 tonnes, coal is also needed in quantity up to 1 tonne and 100 kWh of electricity is consumed, these alone emits 0.8-1 tonne of CO_2 into the atmosphere (Bernard de Quervain 2011). Researchers are therefore being challenged to proffer solution(s) to the reduction of the carbon footprint from OPC production by means of substitution which involves alternating OPC with environmentally friendly materials.

Cement is a crucial component of infrastructure development and an influential material for the construction industry. It is globally used, and hence, contributes from 5% to 8% of the anthropogenic carbon dioxide (CO_2) emissions, and its production utilizes a significant amount of energy (Olivier et al. 2012). The drive to curb CO_2 emission has been on the rise over the years. In order to achieve its reduction, there's need for research focus towards sustainability of cement-based materials and aggregates through recycling of industrial residues or waste materials (Kim and Choi 2012).

Supplementary cementitious materials (SCMs) such as blast furnace slag, mineral wools, fly ash are some of the waste and by-product materials that are conventionally used to substitute some fractions of OPC to enhance the quality of the cement and also make it sustainable or environmental friendly via CO_2 reduction (Lin et al. 2011, Lee et al. 2012). A sustainable cement-based material could be achieved with those SCMs which can serve as a useful means of achieving the goals of the circular economy.

Recently, alternatives to OPC have been well-known in cementing materials produced from alkaline activation of alumino-silicate precursors. These materials exhibit advantageous properties over the constraints of OPC in the areas of reduction in environmental impacts, in terms of CO_2 emissions and energy consumption, and also in durability and mechanical performance (Turner and Collins 2013). The materials are labelled as alkali-activated materials (AAM) or geopolymers (Pacheco-Torgal et al. 2015).

Generally, blast furnace slag, metakaolin or fly ash are raw materials commonly used as a source of alumino-silicates (Xu and Van Deventer 2000). There has been investigations going on in the past few years on the use of industrial and agricultural wastes which have demonstrated their suitability for alkali-activated methods either in a stand-alone or combined setup, for example, as ceramic waste (Reig et al. 2013), sugarcane waste-derived ash (Moraes et al. 2016), fluid catalytic cracking catalyst residue (Tashima et al. 2012), and bottom coal ash (Antunes Boca Santa et al. 2013).

Currently, sodium and potassium silicates are the most common alkali solutions used in activating geopolymer precursors. These silicate solutions are considered the costliest component in geopolymer synthesis and contribute highly to the environmental footprint of geopolymer matrix components (Habert and Ouellet-Plamondon 2016, Habert et al. 2011).

The industrial process of producing the alkali silicates mostly requires high energy cost and generates high CO_2 emissions (Mellado et al. 2014, Gao et al. 2017). The environmental impacts of a geopolymer can be attributed to the precursors and alkali activator, transportation of raw materials, and the thermal and mechanical energy utilized during its production processes, including the curing conditions above ambient temperature. The type and concentration of alkali activator solution has been reported in various life cycle assessments (LCA) as the main contributing factor to the accrued energy and environmental impacts such as the global warming (Habert et al. 2011, McLellan et al. 2011, Heath et al. 2014). The eco-profile assessment of various geopolymers in comparison with OPC concrete, revealed that despite the CO_2 emission reduction, production of geopolymer, however, promotes up to 1000% of some other environmental impacts such as freshwater aquatic ecotoxicity potential (FAETP), mainly as a result of the production of water glass chemically known as sodium silicate (Na_2SiO_3) (Habert et al. 2011).

Over the last two decades, several studies have come up with alternative materials, with interest in establishing the use of industrial by-products and waste materials, as well as, minimise the cost of producing geopolymer binders, which has necessitated the promotion and development of alternative alkali-activators, to be used in combination with the amorphous silica derived from the waste material, this combination can be similar or even more effective compared to the soluble silicate alkali activator (Bernal et al. 2012, Rodríguez et al. 2013, Puertas and Torres-Carrasco 2014). Rice husk ash (RHA) which is an agro-industrial waste, has been found to have a high potential for use as source of silica

for alkali activation (Bernal et al. 2012, Bouzón et al. 2014, Kim et al. 2014). The use of these alternative alkali activators with industrial by-products and waste materials in concrete production shows more environmental and technical advantages compared to OPC (Duxson et al. 2007, Van Deventer et al. 2012). The technical literature often refers a major advantage of these materials to their ability to curtail greenhouse gas (GHG) emissions up to 40-80%, also, the re-use of industrial by-products and /or waste materials as the main materials for producing geopolymer binders (Habert et al. 2011, Davidovits 2008, McLellan et al. 2011, Bernal et al. 2016). A study by Mellado et al. has shown that the use of an alternative sodium silicate from rice husk ash (RHA), has the potential to reduce GHG emission by 63% (Mellado et al. 2014).

Therefore, in this study, the use of industrial residue from the desulphurization process in steel making as an alternative alkali activator for blast furnace slag (BFS) and Stonewool (SW) is investigated.

1.2 Aims

To produce a sustainable geopolymer mortar using desulphurization dust (De-dust) produced as a waste material in steelmaking processes as an alternative alkali activator in lieu of commercially available sodium hydroxide.

1.3 Objectives

This study has been planned to achieve the stated objectives:

- To determine the effect of different dosages of BFS and SW on the properties of the binder
- To identify the workability of various ratios of De-dust against BFS and SW and the effect on the compressive strength of the product
- To analyse the effectiveness of chelating additive (TIPA) on reactivity and properties of the mortar

Overall, this study focuses on the possibility of using solely wastes and industrial by-products to produce alkali-activated mortars in a sustainable pathway with little or no impact on the environment.

2 Literature review

2.1 Concept of alkali-activated materials (AAMs)

Geopolymers are a special case of alkali-activated materials made up of natural source materials or industrial process residues with low calcium content. They are classified amorphous to semi-crystalline and are commonly known as 3-dimensional aluminosilicate materials produced by first activating with an alkali, then curing at a low to moderate temperature for aluminosilicates.

Generally, geopolymer is identified as an amorphous alkali aluminosilicate mostly used in alkali-activated cement, inorganic polymers, alkali-bonded ceramics, geocements, and hydroceramics and they all have the same formation chemistry (Duxson, Fernández-Jiménez, et al. 2007).Geopolymers are formed by the co-polymerisation of single alumino and silicate species which results when a source material containing silicon and aluminium is dissolved in the presence of soluble alkali metal silicates, hydroxides, or alkaline carbonate solutions, at high pH. The chemical composition of geopolymers and zeolites has some resembling characteristics, but the former exhibits amorphous microstructure. Products of geopolymerisation can be characterized by strong chemical and physical properties such as acid resistance and fire and can remodel a variety of alumino-silicate materials into construction and mining materials (Xu 2001).

According to Van Jaarsveld et al. (1997), geopolymerisation can result from any material containing Silicon and Aluminium, which will yield polymeric Si-O-Al-O bonds when a chemical reaction occurs between highly alkaline conditioned silicates and an IV-V fold coordination Al^{3+} as seen in the two reaction pathways in fig 1 below:

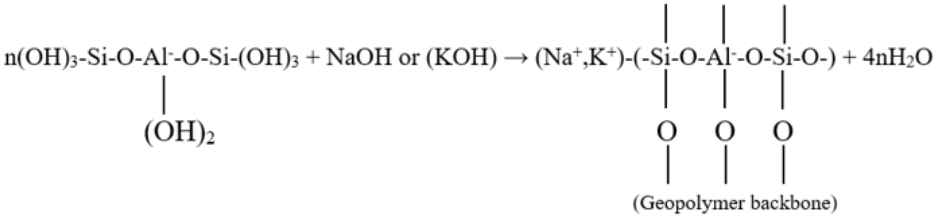

(1)

$$n(Si_2O_5,Al_2O_2) + 2nSiO_2 + 4nH_2O + NaOH \text{ or } (KOH) \rightarrow Na^+,K^+ + n(OH)_3\text{-}Si\text{-}O\text{-}Al^-\text{-}O\text{-}Si\text{-}(OH)_3 \quad (2)$$

(Si-Al materials)

$(OH)_2$

(Geopolymer precursor)

Figure 1. Reaction pathways of geopolymerisation (Van Jaarsveld et al. 1997).

Similarly, Komnitsas (2011), explained that rapid dissolution of aluminosilicates yields $[SiO_4]^-$ and $[AlO_4]^-$ tetrahedral units in solution, the occurrence of this reaction requires a high alkaline condition. The tetrahedral units formed gets to distribute oxygen atom, thus, linking up to the polymeric precursor and forming polymeric Si-O-Al-O bonds as seen in the two reactions below, Fig. 2;

$$(Si_2O_5.Al_2O_2)n + H_2O + OH^- \rightarrow Si(OH)_4 + Al(OH)^{4-} \quad (3)$$

$$Si(OH)4 + Al(OH)^{4-} \rightarrow (\text{-Si-O-Al-O-})n + 4H_2O \quad (4)$$

O O

Figure 2. Polymeric bonds of aluminosilicates (Komnitsas 2011)

When this process is used, water is discharged which is used up as the mixture is dissolving. The uniformity of the mixture during handling is achieved with water that was released at the reaction time. Contrarily, in the hydration process of OPC mixture, the chemical reaction of water does not necessarily aid in the workability of the mixture (Singh et al. 2015).

Quite a minimal amount of greenhouse gases (GHGs) particularly CO_2, are emitted during their manufacturing process which also makes use of high valued raw materials, hence presenting AAMs as more economically and environmentally sustainable materials (Provis 2014a, Abdalqader et al. 2016). The stronger and denser structure of AAMs is a result of $SiO^{4-}{}_4$ anion which is an important feature in high-performance AAMs (Pacheco-Torgal et al. 2015, Provis and Van Deventer 2014). The adoption of any aluminosilicate material for geopolymerization synthesis depends on their chemical composition, mineralogical content, fineness and glassy phase make-up, and morphology for their reactivity. In order to produce stable geopolymer, the following essential rules must be considered; the source material should be such that requires a low amount of water, and can easily

release aluminium. Also, the source material should be exceptionally amorphous and its glassy content adequately reactive. Sodium silicate (Na_2SiO_3), sodium hydroxide (NaOH), potassium hydroxide (KOH), and potassium silicate (K_2SiO_3), are the alkali activators used in activating aluminosilicate materials. Sodium hydroxide exhibit a high potential capable of releasing silicate and aluminate monomers (Duxson, Fernández-Jiménez, et al. 2007).

According to Duxson et al. 2007, factors affecting the properties of geopolymer are;

- Careful collection of the raw materials
- Adding an accurate amount of mixtures and mixing properly
- The processing method must correspond to a specific application

Compared with calcium-rich slags alkali activation, geopolymerization of metakaolin/fly ash produces reaction product like that of zeolite, that is, sodium aluminosilicate hydrate gels made up of different ratios of Si/Al, while in calcium-rich slag activation, the dominant feature is calcium silicate hydrate which consists of a low Ca/Si ratio (Singh et al. 2015). The advantage of metakaolin-based geopolymer is that its overall synthesis be done routinely and certain properties such as high specific area, strong absorbability, porosity, and coordinative solid stimulated bonds (Cheng et al. 2012), can be used during the setup and development. Its disadvantage is as a result of its plate-shaped particles which inhibits the rate of flow of the mixture, making the process more complex and requiring additional water (Li et al. 2010b). Duxson et al. 2007, however, explained that the strength and durability of the fly ash-based geopolymer are generally higher than that of metakaolin-based geopolymer. Whereas, high early strength and outstanding acid resistance is associated with slag-based geopolymer than those of fly ash-based and metakaolin methods (Singh et al. 2015). There are variations in the chemical properties and microstructures of geopolymer prepared from different aluminosilicates, even though their physical properties are seemingly alike.

Considering the advancement in alkali-activated cements, the phase composition of their hydration products has been earmarked as the basis for their classification, the aluminosilicates are classified based on R-A-S-H, where R is Na+ or K+, while the alkali-activated slag or alkali portland cement are classified based on R-C-A-S-H (Krivenko and Kovalchuk 2007). As a result of the early compressive strength, exceptional chemical resistance, outstanding fire resistance, and low permeability properties of geopolymer, significant attention have been drawn to these binders (Provis and Van Deventer 2009).

Since two decades ago, the possibility of using AAMs as a sustainable substitute in making binders for OPC or concretes, has attracted the attention of scientists on research and advancement of AAMs (Pacheco-Torgal et al. 2015, Provis and Palomo 2015). The main precursors for obtaining AAMs are; Steelmaking industry by-products such as BFS, by-products from coal combustion that is, fly-ash, and natural clays such as kaolinite (Duxson and Provis 2008). These precursors are more effective when used as co-binders, because when blended and activated, they exhibit strong mechanical strength, though depending on the activation condition because the quality of the silicate species at the early stage of the reaction process is modified by these conditions (Bernal, Rodríguez, et al. 2011). Also, a preliminary study by (Alzaza et al. 2019, Kinnunen et al. 2017, Yliniemi et al. 2016) narrated the use of rockwool (RW) as a precursor for alkali activation in producing AAMs.

The various outlined advantages exhibited by geopolymer properties shows its potential as an alternative to OPC for the production of different sustainable products capable of being used as fibre-reinforced composites, building materials, fire-resistant coating, and so on.

2.2 Components of geopolymer matrix

This section outlines the various materials (aluminosilicates) used in preparing geopolymer binders and how they affect the quality of the product. These materials are of two categories: precursors (Mainly industrial by-products and waste material) and alkali activators. In some cases, additives constitute part of the mixture components especially when the matrixes are made up of dry components.

2.3 Precursors

An increasing major environmental concern is focused on industrial residues and their various storage conditions, precisely in Europe, as stipulated by the Council Directive 1999/31/EC, also their limit values given by the Council Decision 2003/33/EC. These concerned waste materials are of low commercial value because their reuse is unachievable, and have strict requirement for its proper disposal, hence, generating economic and environmental worries. It is therefore imperative to establish applicable means to use a

substantial amount of these residues back to the production chain as this would reduce financial and environmental costs, and as well converting them into technically efficient materials similar to the present circular commodities.

The European Union legislation has stipulated that by 2020, 50% of industrial waste should be processed to be reused, recycled or recovered. This legislation aims specifically to ward off waste generation (De la Paz 2014). An efficient means of waste treatment is via material recycling, energy recovery is considered the second-best, while the disposal is seen as the least useful option (Meinander et al. 2012). A very large percentage of various by-products and waste materials can be utilized in the construction industry as a partial replacement for cement or aggregate, filling of hill sight, the foundation for road and railway pavements. Common examples are fly ash (Deschner et al. 2012), blast furnace slags (Maghool et al. 2017), construction and demolition wastes (CDW) (Avirneni et al. 2016).

The alkaline activation system outlines an effective means that continuously and strongly promotes the standard of building with recycled materials. In the alkaline activation of geopolymer materials, the solid precursor(s) that are highly embedded with silica and alumina, with an outstanding level of amorphization is required. Studies conducted by Fernández Jiménez et al. (2013) and Martin et al. (2015) revealed that some varieties of applications can be prepared using alkali-activated materials, hence, substituting ordinary Portland cement (OPC). The use of waste and /or industrial residue is attracting a large number of researches to ensure environmental sustainability as the waste materials could have a high polluting capacity despite their usefulness.

This study is one example of such describing the utilization of these materials and promoting environmental sustainability, as the precursor materials used were solely waste and industrial residues such as stonewool from construction and demolition waste, blast furnace slag and desulphurization dust both from the metallurgical processing industry.

2.3.1 Mineral wool

Over a decade and a half, the European Commission has slated construction and demolition waste as one of the six priority waste streams (Papatzani and Paine 2015). Recently, prioritization based on the elimination, prevention, and reuse of materials was given by

the recent Waste Framework Directive (European Commission 2012, European Commision 2015). Indeed, Europe records yearly, 850 million tons of generated CDW (Tošić et al. 2018). Even though this trend is decreasing, yet it persists in generating grave environmental problems because the amount of this waste recycled is only half percent of the total generated (Villoria Sáez et al. 2012).

According to (Soutsos et al. 2011, Bourguiba et al. 2017), there has been an acceptable solution for reassessing and recycling of CDW in the recent years, due to the partial replacement of the raw materials for construction purposes with CDW. The current regulations for energy saving has recently initiated an increase in auditory and thermal requirements, hence, resulting in an increase in mineral wool waste from home insulations (Papadopoulos 2005), and as such, mineral wool has been recorded as 0.2% of the amount of all CDW generated (Väntsi and Kärki 2014), which justifies 60% of the number of insulation materials utilized in construction. In the year 2020, as seen in Fig. 3 below, 3,5 million tonnes of mineral wool have been projected to be produced in the EU27 countries.

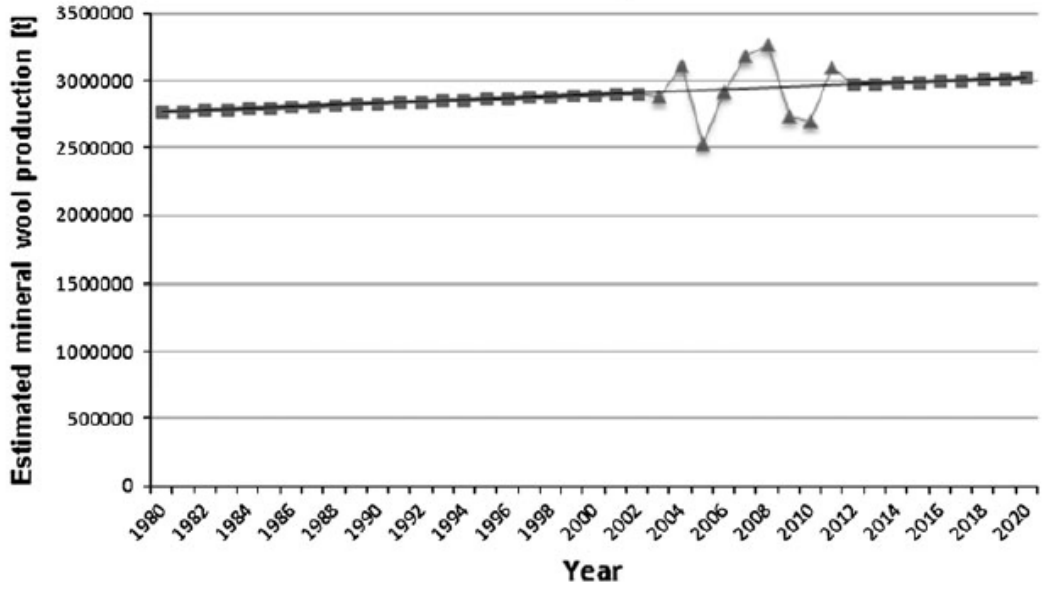

Figure 3. Estimated volume of mineral wool production in EU27 countries between 1980-2020 (Väntsi and Kärki 2014).

Calculating the amount of this waste precisely seems difficult as the reuse, recycling or recovery percentage is yet uncertain, however, the model given by Väntsi 2014, estimated that in 2020, within the EU-28 zone, above 2.5 million tonnes of mineral wool will be generated. The recyclability of mineral wool is considered quite low, but its percentage can be increased by reusing the waste material (Väntsi and Kärki 2014), therefore, the

benefits of reducing CDW has necessitated the consideration of mineral wool waste for reuse in cement composites (Hagerman 1987, Cheng et al. 2011, Lin et al. 2012), fiber-based composites (Felaji and Kehrer 1990), ceramics (Kizinievič et al. 2014, Pranckevi 2011), tiles (Dunster 2007), gypsum board (Cadotte 1970, Ali 1985, Long 1985), briquettes (Heinelt 1996, Talling and Sarudis 1995), and recently in geopolymers (Yliniemi et al. 2016, Kinnunen et al. 2017).

The principal type of mineral wool produced is rockwool, accounting for 70% of the total mineral wool production, while the use of slag wool has drastically dropped, the quantity of glass wool (GW) manufactured is roughly 1/3 of the total of RW produced (Müller et al. 2009).

Rockwool is an inorganic material made up of fibres, it is made by spinning molten material while letting a blast of steam pass through it. Rock wool is commonly used as an insulation for acoustic purposes, pipe insulation, protection of fire, cement supplement, and even as synthetic soil for plant growths (Jiřičková and Černý 2006). The low-density nature of RW makes it difficult to recycle as it would require large landfill areas, making it environmentally unfriendly, coupled with transportation issues. Hence, using it in the concrete industry as a partial substitute for aggregates or cementitious materials could help solve the recycling problem. Although, the chemical composition and particle size of the by-product plays an important role in this means. According to Cheng et al. 2011, a pozzolanic product with an improved properties can be obtained when a rock wool waste having a particle size distribution between 17 to 250 mm is used as an alternative for coarse or fine aggregates, the study revealed the feasibility of ground rock wool waste to be used as a partial replacement for aggregates in cement-based composites which is attributed to its chemical composition and physical properties.

2.3.2 Blast furnace slag

Blast furnace slag is an industrial by-product which is produced during the manufacturing of pig iron when coke reduces the iron ore in the temperature range of 1350 ºC-1550 ºC in a blast furnace (Kolani et al. 2012), comprising mainly silicates and alumino-silicates of calcium including that of other bases, which are consistently produced with iron in the blast furnace via combustion. Through the ore, molten iron which is the main product of

the blast furnace is extracted while the rest of the components forms a liquid slag called molten slag. This molten slag is then cooled rapidly by quenching with a large amount of water either in a pond or with powerful water jets, which turns into near fully noncrystalline fine granular called granulated slag having a large amount of amorphous state silica and alumina (Sadek 2014). The sand-like granules are overall grounded to a fine powder called ground granulated blast furnace slag (BFS). This finely ground slag is known to exhibit latent hydraulic cementitious qualities and therefore, has been significantly used as a commendable substituted material for Portland cement (Alp et al. 2008, Tsakiridis et al. 2008), as a result, up to 47.5% CO_2 emission reduction is achieved when cementitious slag percent from 2.83% to 10.3% is substituted in cement production (Crossin 2015).

Grinding of BFS requires approximately 10% of the total energy needed for Portland cement production (Shi and Qian 2000). The quantity of BFS usually blended is about 25-30% in regular cement (Fu et al. 2000). It is possible to replace cement with BFS from 30% up to 85%, but most applications often require 50% (Siddique and Khan 2011), considerations and method for high-volume replacement has been of significant interest lately (Rashad and Sadek 2017).

The particle size distribution of the slag after milling, its glass content and chemical composition determines the activeness of blast furnace slag (Liu et al. 2019). Concretes made with BFS are less sensitive to early-age thermal cracking due to generated heat of hydration (Turu'allo et al. 2013). The hardened concrete has a denser microstructure with smaller and fewer capillary pores, resulting in an enhanced ability to withstand chemical attacks (Heikal et al. 2014).

Iron slag production was globally projected to grow between 300 to 360 million tonnes in 2015 (Kimball, 2016). An increase in global iron production and increasing economic development has led to a high rise of slag, causing more of it being disposed of in landfills. Environmental pollution and landfill disposal of slag can be averted by reusing it as a valuable resource especially when finely granulated. A sustainable way of doing this is to incorporate slag in construction materials.

In alkali activation, BFS is the most extensively used precursor. The main components of its properties are CaO-MgO-Al_2O_3-SiO_2 (Li et al. 2010a). The principal reaction product

during alkali activation of BFS is a crystalline hydrated calcium-silicate (C-S-H) gel having a low C/S ratio nearly at one (Fernández-Jiménez et al. 2003, Escalante-Garcia et al. 2009). And there has been a comprehensive review of these binders predominantly for use in construction purposes (Palomo et al. 2014). A recent study by Özbay et al, 2016, has further showcased the environmental benefits of using BFS, according to the study, energy-saving, conservation of natural resources, and carbon dioxide emission reduction can be achieved by using BFS in constructions.

2.4 Activators

Activators are used in the preparation of geopolymer binders so as to help enhance their mechanical strengths. These activators are generally known to be alkaline in nature, hence, they are called "alkali activators". They are of different types and are available either as commercial products or industrial by-products/wastes.

Generally, the activators mostly used are usually alkali hydroxides and silicates such as:

- Sodium hydroxide (NaOH)
- Potassium hydroxide (KOH)
- Sodium and Potassium silicate which can be obtained as a water glass, example $Na_2O{\cdot}nSiO_2{\cdot}mH_2O$
- Sodium Carbonate (Na_2CO_3)

2.4.1 Sodium hydroxide

Sodium hydroxide (NaOH) is produced as a solid by the electrolysis of sodium chloride solution, which produces NaOH, hydrogen, and chlorine. The molarity of NaOH solution required for alkali activation is achieved by dissolving the solid NaOH in water. Its concentration is considered an essential factor in the synthesis of geopolymers (Puertas et al. 2000), as it clearly affects both the microstructure and compressive strength of geopolymer (Somna et al. 2011), thus, the higher the concentration of NaOH, the higher the compressive strength of geopolymer concrete (Hardjito et al. 2004), and due to the high solubility rate of Al^{3+} and Si^{4+} in NaOH solution, the ease of dissolution of minerals increases (Xu and Van Deventer 2000b). However, high amount of sodium in the

geopolymer synthesis may result in efflorescence. Xu and Deventer found that the rate of dissolution of minerals was generally higher with NaOH solution than with potassium hydroxide (KOH) solution (Xu and Van Deventer 2000). Activating a high CaO material (example BFS) with NaOH shows more significant dissolution of Ca and Mg ions in the slag and formation of a low c/s ratio (≈ 0.7-0.9) honeycombed C-S-H- gel type, compared to activating with KOH activator which dissolves less Mg (Garcia-Lodeiro et al. 2014).

2.4.2 Potassium hydroxide (KOH)

KOH which is produced via electrolysis of potassium chloride solutions, produces concrete with several properties such as quicker reaction, minimal strength, and homogenous microstructure, this is different when sodium silicate is used. Also when compared to water glass, KOH activator produces binders with high compressive strength within 24 hours of casting, although after one day, strength development reduces significantly (Brough and Atkinson 2002). The ionic size of KOH and NaOH creates the variations in their activeness. The ionic size of Na^+ (116pm) is smaller compared to K^+ (152pm), hence, Na^+ is more active in affecting the process of dissolution of aluminosilicates minerals (Xu and Van Deventer 2000b).

2.4.3 Alkali silicates

Sodium silicate which is manufactured via melting of silica sand and sodium carbonate, can significantly increase the compressive strength of a concrete when combined together with sodium hydroxide, as an activator (Hardjito et al. 2004), the binding ability of sodium silicate, its availability, and adhesive properties, makes it a useful activator in geopolymerization (Dimas et al. 2009). When water glass is used in slag activation, it promotes strength development by acting as an alkaline activator and an influencer of high silica primary gel formation. The emergence of this gel occurs during the reaction of soluble silicate with Ca^{2+} ions in the slag, forming a C-S-H/C-A-S-H-type, calcium silicate hydrate and silica-rich (Garcia-Lodeiro et al. 2014). It is possible to use only silicate solutions as an alkaline activating solution, although the activation process in most geopolymer studies have concentrated on using silicate solution with alkali solution (Memon et al. 2011, Görhan and Kürklü 2014), because the silicate solution yields silicate ions in

aqueous phase, and aid the activation of the precursors, hence, enhancing the dissolution process and yielding products with good mechanical properties (Rees et al. 2004).

At equal concentration, the viscous nature of potassium silicate appears slightly higher than that of sodium silicate, although they exhibit similar physical properties, but potassium silicate tends to be more reactive due to its high solubility and does not cause efflorescence even at high temperatures (Vickers et al. 2015). However, sodium silicate is less expensive than potassium silicate.

2.4.4 Alkali carbonates

According to Garcia-Lodeiro at al. (2014), geopolymers produced with Na_2CO_3 activator are associated with lower environmental impact compared to those produced with silicate or hydroxide solution, which explains the interest in Na_2CO_3 activator, as it also produces a lower pH compared to other alkali-activated binder systems, this is seen as a potentially favorable effect with regards to occupational health and safety. However, academia and relevant industries show less attention to carbonate-activated binders than other systems, because in most cases, they harden and have very low rate of strength development than sodium silicate or sodium hydroxide activated cement (Garcia-Lodeiro et al. 2014). Generally, preference to sodium-based-alkali activators is attributed to their high reactivity, low cost, and availability (Provis 2014b), but for high-temperature applications, potassium-based alkali activators are usually suggested as activators (Barbosa and MacKenzie 2003).

In the production of AAMs, a liquid solution of these activators is normally added to the product mixture. Alternatively, dry powder-like alkali content material(s) could be used to serve the same purpose and can be mixed or combined with the precursors (Carrasco and Puertas 2017, Luukkonen et al. 2018, Adesanya et al. 2018). Aluminosilicate materials such as BFS, fly ash, etc. can be effectively activated using alkali hydroxide ROH, silicic salt ($R_2O.nSiO_2$) and in silicic salts of weak acid (R_2CO_3, R_2S, RF), in these cases, R represents either K, Na or Li which are alkali metal ions (Hardjito et al. 2004, Kovalchuk et al. 2007).

Other compounds also used is Na_2SO_4, which can also serve as a useful activator for the production of mixed cement containing a considerable amount of Portland cement, or

activating calcium-rich precursors like BFS (Shi et al. 2006, Bernal 2016). Other potential activators include MgO, CaO and either $Ca(OH)_2$ (Provis 2018).

Criado et al. reported that the dissolution of BFS is aided by alkaline activators with high pH and that this enhances strength development and chemical reaction (Criado et al. 2018). In addition, activating slag with silicate yields concrete with good stability and enhances mechanical properties, compared to activating with sodium hydroxide (Wang et al. 1994). Also, activating BFS with Na_2SiO_3 results in increased heat of evolution which heightens as water to binder (w/b) ratio reduces, and when w/b ratio goes up, the heat also reduces, the reverse is seen when NaOH activator is used, producing heat of hydration that is close to that produced by OPC pastes (Shi et al. 2003). The composition of these alkali activating material(s) influences the activation procedure, for example in slags and fly ash precursors where the consideration to the impact of the cations-anions, and pH effects are evaluated. (Carrasco and Puertas 2017).

2.4.5 Alkali activation of stonewool

In 2017, Kinnunen et al., found RW to be a perfect precursor for geopolymerisation with regards to the mineralogy and chemical make-up. The solubility of the soluble elements (aluminium and silicon) of RW however, does not deter it from irregularities during geopolymer synthesis, its physical structure brings about more difficulty due to its wide fibre size of 5 to 10µm, and as a result, a substantial amount of RW added to the matrix obstructs the flowability of the paste (Kinnunen et al. 2017). Increasing the amount of water to aid the flowability of the paste does not proffer solution to the difficult challenge, instead, it causes the product to crack and reduces the compressive strength, which is attributed to the loss of the excess water during curing. Therefore, these challenges associated with the use of rock wool are controlled by making available, a high pH concentration, where the rockwool fibres which had already been gently dissolved in an alkali solution, is vigorously mixed via mechanical forces and cured at slightly high temperatures of about 50^{o}C. This solution reveals the feasibility of the use of rock wool in AAMs, as it enables an adequate amount of solid rock wool content in the geopolymer matrix (Kinnunen et al. 2017).

The consistency of the chemical and physical properties of mineral wool has presented it as a suitable raw material for alkali activation. The high silica content and x-ray amorphous mineralogy of RW contribute to its potentiality as AAM (Yliniemi et al. 2016). The reactivity of the high content of Ca and Mg in RW has been revealed in previous studies (Bernal, Provis, et al. 2014, Bernal, San Nicolas, et al. 2014, Walling et al. 2015), although Yliniemi et al. (2016) found only new phase of Mg in alkali-activated RW samples where phases of sodium aluminate silicate hydroxide hydrate and magnesium aluminium hydroxide carbonate were identified, alongside the amorphous phase. Kinnunen et al. (2017) also found a NASH phase when RW was activated with sodium aluminate solution.

An advantage of using RW as a co-binder can be attributed to its ability to act as a CO_2 sorbent due to the reaction of its Mg content with CO_2 when a hydrotalcite-type magnesium phase is formed, this type of reaction was reported in a study by (Yliniemi et al. 2016), it was also observed from the study that alkali-activation of RW with sodium aluminate produces binders with maximum compressive strength of 30.0 MPa and maximum flexural strength of 20.1 MPa, which shows that RW has a huge capacity to be utilized as precursor in alkali activation-synthesis even without a co-binder.

2.4.6 Alkali activation of BFS

There are various chemical factors regulating the reaction mechanism of slag activation which aids in the build-up of resistance and durability of the activated pastes. These factors are categorized based on their association to the activator used in the reaction process, and to the features of the precursors in use (Carrasco and Puertas 2017).

AAMs such as alkali-activated slag (AAS) and alkali-activated slag concrete (AASC) are produced by the activation of a granulated BFS with an alkali. Mixing BFS with water results in a low rate of hydration and slow strength development, therefore, exposing the mixture to an alkaline activator increases the hydration reactions and activates a high pH environment. Different alkaline compounds such as sodium silicate (Na_2SiO_3), sodium hydroxide (NaOH), sodium carbonate (Na_2CO_3), potassium hydroxide (KOH) are used either separately or combined, to activate slags. With regards to increasing in compressive strength of the BFS slag precursor, sodium silicate is considered a more productive activator amongst others, as up to 100 MPa of one-part alkali-activated slag mortar strength is obtained at 28 days (Luukkonen et al. 2018).

2.4.7 Characterisation of alkali-activated BFS

In order to use BFS in alkali-activation, it needs to be quenched (i.e granulated and pelletized), then ground to produce a reactive material. Due to the rapid hardening of AAS, retarders could be used to control the rate at which it sets (Pu et al. 1992, Yang et al. 2011). Calcium Aluminosilicate Hydrate gel (C-A-S-H) is the main product from the activation of BFS, it resembles the gel produced in the hydration of OPC (C-S-H), but has a lower CaO/SiO_2 ratio (between 0.0 and 1.2) than that of C-S-H which has CaO/SiO_2 ratios between 1.5 and 2.2. The product of this reaction can result in the formation of by-products like the hydrotalcite ($Mg_5Al_2CO_3(OH)16.4H_2O$) when there is a high content of MgO in AAS synthesis (Haha et al. 2011), and also formation of zeolites, for example gismondine, as a result of high amount of Al_2O_3 and low MgO less than 5% are involved in activation of BFS (Bernal et al. 2010, Bernal, Provis, et al. 2011). The type of activator used determines to a large extent, the composition and configuration of the C-A-S-H paste produced after activating the slag (Aydın and Baradan 2014).

High mechanical strength and durability are other distinguishable features of AAS (Fernández-Jiménez et al. 1999, Rashad 2013). Hydration products of AAS are known to form quite early, within 24 hours. It undergoes different stages of formation within the one-day period; dissolution, followed by precipitation, and then solid-state.

There is a tendency of Chloride test results of an AAS to be affected due to the existence of Na^+ and OH^- in the pore solution (ASTM C1202), this is because there is a chance for NA^+ to obstruct diffusion while the Cl- ions are driven electrically into the pore network, causing the charge transfer to enlarge while the test runs (Bernai et al. 2013). As a result, Shi 2004 reported that the chloride test of an adequately cured AAS concrete had shown a low chloride permeability compared to concretes made with OPC.

2.4.8 Alkali-Activation Pathway

Production of alkali-activated binders can be done through two major pathways (Provis 2018);

- One-part mix which involves mixing the dry precursors with water
- Two part-mix, where a liquid activator is added to the dry powder(s)

Most AAMs already in use were produced using the two-part mix pathway, and it is likely to get to the market first. Although, the one part-mix which is mostly produced and packaged from the factory, has the potential of becoming a measurable technology if its value becomes adequately enhanced and solution to its sluggish increase in strength is established. The scalability of a two-part mixture type could be feasible in precasting where control for chemical handling and curing times are implemented (Provis 2018).

There is an environmental advantage associated with geopolymer cement produced with a one-part mix pathway. Generally, its contribution to the global warming potential is less than 5 % for cement produced with 100 % OPC, and also with economic allocation, it enables achievement of 80 % global warming potential reduction (Habert and Ouellet-Plamondon 2016). Recently, Wagner company applied a one-part geopolymer in the construction of a four-storey building at the University of Queensland (Aldred and Day 2012).

Production of one-part mix pathway can be done by intergrinding or cocalcination of two or more precursors (i.e., aluminosilicate powders) and the solid alkali activator which could either be alkali silicate, hydroxide or carbonate (Gluth et al. 2013, Ke et al. 2015, Adesanya et al. 2018,). Fig. 4 below shows the dry mixing method used in the production of one-part AAMs.

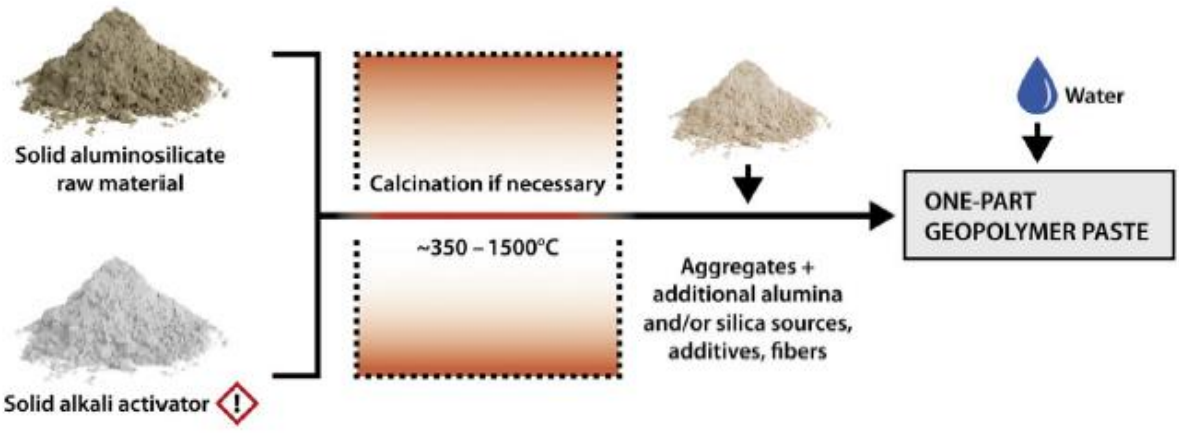

Figure 4. Preparation procedure of one-part alkali activation pathway (Luukkonen et al. 2018)

Addition of water to one-part geopolymer mixture leads to the following four actions (Matalkah et al. 2017):

1. ion exchange

2. hydrolysis
3. network breakdown
4. release of Si and Al

These four reactions result in formation of gel/(geo)polymerization.

While the actual steps in two-part geopolymers are: speciation, gelation, reorganization and polymerization, which are the next reaction steps of one-part geopolymers after the initial four main steps (Duxson, Fernández-Jiménez, et al. 2007). The accessibility of Si and Al from the geopolymer precursor(s) and their rate of release are two major differences between one and two-part geopolymers (Luukkonen et al. 2018b). The availability of Si was found low in one-part geopolymer due to the heterogeneous structure of the crystalline phase, making its reaction slower than the soluble silicate solution used in two parts geopolymer (Hajimohammadi et al. 2011). The rate of release of alumina was, however, observed faster, triggering a rapid formation of Al-rich gel, before the formation of silica-rich gel, and as a result, forming a homogenous geopolymer gel structure (Hajimohammadi et al. 2010), they also observed that the concentration of the dissolved alumina was originally high which led to obstruction of the dissolution of silica, causing the binder to develop a high strength at the early stage of curing, but having lesser strength in the later stage. Therefore, Duxson and Provis 2008b, considered alumina as the major important factor that can influence the following geopolymer properties: acid resistance final strength enhancement (final strength), setting time, microstructure, and flexural strength.

Ke et al. (2015) and Sturm et al. (2016), came up with findings that presented N-A-S-(H) gels as the binding phases of one-part geopolymers, this phase is formed after the addition of water and curing. Also, this one-part geopolymer has hydratable iron minerals, aluminium, and magnesium as components of its reactive minor phases (Peng et al. 2017).

2.4.9 Challenges of alkali activators in AAMs production

Challenges associated with the use of alkali activators in producing AAMs could be classified based on economic and environmental impacts. Ordinarily, activators are prepared

using first-grade commercial reagents, mainly sodium or potassium hydroxide, and sodium or potassium silicate. The use of these reagents, unfortunately, attracts a high financial cost, and their production process generates a large amount of CO_2, thereby, devaluing and defeating the essence of using industrial residues as precursors, which is "environmental well-being" (Cristelo et al. 2015).

Geopolymer based concrete produced with sodium silicate solution has been found to have higher environmental impacts than OPC (Habert at al. 2011), the environmental impact categories are shown in Fig. 5 below.

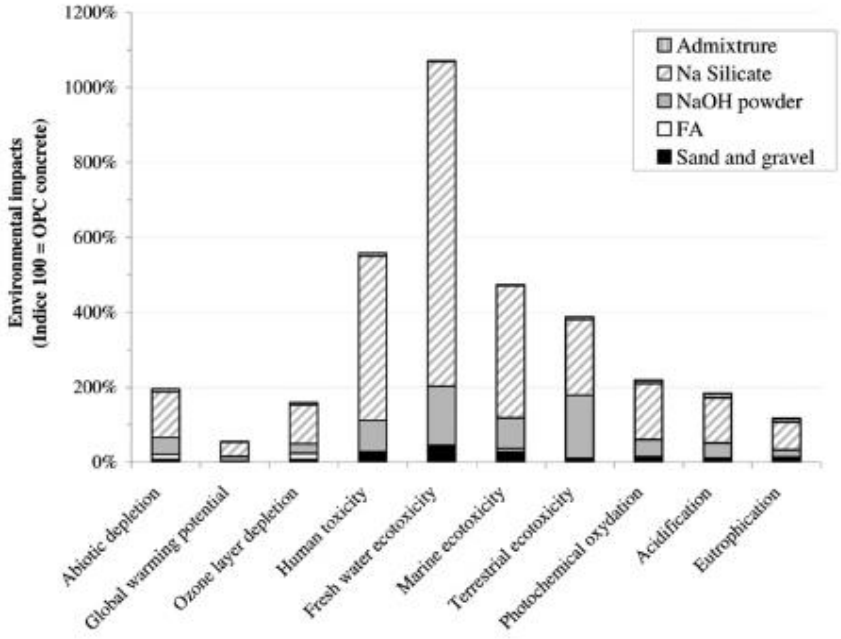

Figure 5. Environmental impact categories of geopolymer based concrete (Habert et al. 2011)

According to life cycle assessment (LCA) reports, the type and concentration of alkali activator solution affects the energy embodied in these binders and their environmental impacts such as the global warming potential (Habert et al. 2011, McLellan et al. 2011, Heath et al. 2014).

Environmental impacts are associated with alkaline activating reagents which stem from the production of reagents needed for their preparation. Comparison between geopolymer concrete and OPC concrete estimated a 320kg $CO_2{}^{-e}m^{-3}$ of $CO_2{}^{e-}$ footprint generated by concrete produced with geopolymeric binders, which although 9% less than 354kg $CO_2{}^{-}$

$^{e}m^{-3}$ of $CO_2{}^{e-}$ generated by OPC concrete, but the unexpected higher emissions of geopolymer concrete was attributed to raw material transportation and significant use of energy during manufacture of alkali activators of geopolymers, mining treatment, and the high curing temperature which is required so as to achieve geopolymer concretes with appreciable strength (Turner and Collins 2013).

Challenges associated with alkali hydroxide solutions are attributed to their high alkaline nature which makes it difficult to handle, thereby posing health and safety risks (Vinai and Soutsos 2019). Disadvantages of NaOH is related to its corrosive and hygroscopic nature, and the formation of sodium carbonate when in contact with CO_2 (Luukkonen et al. 2018). The rate of production of NaOH presently, is approximated to 60 Mt annually, and it is produced through the Chlor-alkali process, it is not beneficial to increase the production size because it produces chlorine as a by-product which has limited world-market value (Provis 2018, Davidovits 2015).

According to Passuello at al, characterization of geopolymer synthesis materials in terms of ecotoxicity such as freshwater aquatic ecotoxicity potential (FAETP), marine aquatic ecotoxicity potential (MAETP), terrestrial ecotoxicity potential (TAETP), and human toxicity potential (HTP), appeared unsuitable particularly due to the use of NaOH (Passuello et al. 2017), they also observed that the highest contribution to the life cycle of geopolymers is credited to the environmental impact associated to the production of NaOH and commercial sodium silicate (water glass). The thermal (furnace) process of producing commercial water glass is done via direct melting of pure silicon sand and soda between 1100 ºC - 1200 ºC (Zah and Hischier 2007), while the hydrothermal process involves the use of an autoclave, where sand is dissolved in NaOH solution around 180 ºC – 300 ºC (Trabzuni et al. 2011). A large amount of CO^2 is emitted through these industrial processes.

The use of sodium silicate as an activating solution in alkali activated binders,supplies the reactive part of silica that is essential and generally used together with sodium hydroxide to produce the activator (Provis and van Deventer 2014, Pacheco-Torgal et al. 2015a). The production of sodium silicate via melting of quartz sand and sodium carbonate at elevated temperatures of about 1400 to 1500 ºC, consumes between 420 and 1250 MJ/ton of energy and results in the emission of a total carbon dioxide of 403 to

450kg/ton (European Commission 2007). In addition, producing one ton of silica equivalent from commercial sodium silicate has been estimated to cost above 2100 USD (Lázaro García 2014). Therefore, the major drawbacks on the use of sodium silicate solution are attributed to its expensive nature, and because it is the leading greenhouse gas emitter amidst other materials, making it the costliest and highest environmental footprint material in the production synthesis of AAMs (Habert et al. 2011, McLellan et al. 2011, Turner and Collins 2013, Nazari and Sanjayan 2016). The total greenhouse gases present in an AAM concrete layout is about 50-70% of the emissions from sodium silicate production, the dissolution of silica and sodium carbonate contained in the raw material up to until 1400^{o}C to yield the sodium silicate is considered the reason for such high value of GHG (Turner and Collins 2013).

Heath et al. 2014 reported that the ratio of SiO_2: Al_2O_3 during alkali activation of geopolymer is the most crucial factor in determining the global warming potential (GWP) of activators, the report shows that the ratio of SiO_2:Al_2O_3 above 3.5-4.0:1 has a higher GWP (Heath et al. 2014).

Due to these economic and environmental disadvantages of sodium silicate as an activating agent in AAMs, evaluation of other sustainable means of obtaining silica for producing an activating solution has become one of the important research focus (Provis 2018, Provis and Palomo 2015). Also, Na_2CO_3, obtainable from trona (Na_2CO_3.$NaHCO_3$.$2H_2O$), material from the geologic origin, has been identified as a valuable activator as NaOH and is used under heat for activating bentonite, albite or kaolin (Feng et al. 2012, Peng et al. 2015, 2017). However, using dolomite and Na_2CO_3 while calcinating aluminosilicate precursors at elevated temperature results in CO_2 emission. Therefore, using an alternative alkali activator that has little or no environmental impact and cheap, but yielding valuable and sustainable products, could be a better solution to these challenges.

2.4.10 Alternative alkali activators

The setbacks in the advancement of AAMs technique as a result of the disadvantages of the alkali activators has necessitated a complete or partial utilization of industrial residues

in producing environmentally friendly and inexpensive alkali activator(s). Recently, researchers have come up with different ways to reuse wastes such that it serves as a source of alkali activator to partially replace the commercial products. One of the preliminary research carried out in 2014 by Puertas and Torres-Carrasco (2014), concentrated on glass waste produced from the industry and urban areas, analysing its potential to be used as an alkali activator for BFS, the findings showed that microstructural development and strength of the pastes that were activated using the glass waste has similar features as those activated with commercial activators.

There are other waste materials that have been evaluated as sources for silica, with advantages in regards to ecological footprint and cost benefits (Carrasco and Puertas 2017). These materials include: rice husk ash from agro-industrial by-product which was used as a complete replacement for commercial sodium silicate for the activation of fly ash and BFS, the findings revealed a 42 MPa mechanical strength AAM produced in 7 days (Mejía et al. 2013). The use of olivine nano-silica as an alternative source of silica in alkali activation of slag-fly ash blends showed that within 1.0 to 1.8 of the activator modulus range, CO_2 emission reduction of 20.4% to 29.0% respectively was achieved (Gao et al. 2017). Also, the use of chemically modified nano-silica in activating fly ash binder has produced binders with mechanical strengths similar to that produced with commercial sodium silicate, it was observed that the need for water and porosity of the samples activated with the nano-silica are lesser compared to samples activated with commercial sodium silicate (Rodríguez et al. 2013). Recently, research was carried out using solely waste/industrial by-product as an activator and precursors, it involved the activator being replaced by a sodium hydroxide waste solution which was earlier utilized in the process cleaning of foundry sand molds generated from the aluminium casting industry, while fly ash and glass powder were used as the precursors, the result showed that the cleaning solution contains soluble tetrahedral aluminium which has the potential of activating low-Al, Si-rich raw materials, consequently, resulting in the achievement of high strength values when used in activating the aluminium deficient glass powder (Fernández-Jiménez et al. 2017).

Aside from CO_2 and cost reduction benefits offered by these alternative activators, other environmental issues that could emanate from depositing these wastes in landfills, is another important advantage of utilizing industrial wastes/by-products as an alternative activator in producing AAMs.

In this study, both the activator and precursors used are wastes and industrial by-products. The precursors in this study are the stone wool waste and BFS, while the desulphurization dust (De-dust) containing a high amount of sodium served as the alternative activator. TIPA was added to increase the dissolution of the elemental components in the mix composition.

Therefore, one-part "just add water" alkali-activation mixing pathway was employed in the paste preparation, using BFS and SW waste as the precursors, and the desulphurization dust as the activating material, while adding different dosages of TIPA.

2.5 Triisopropanolamine (TIPA)

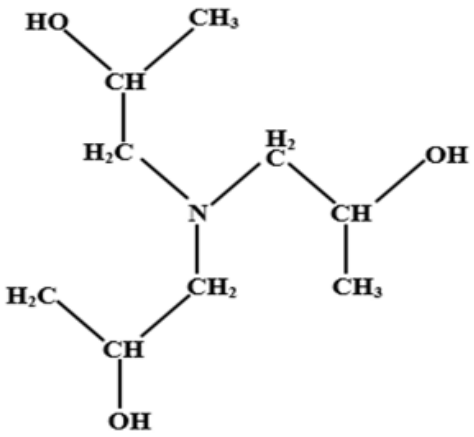

Figure 6. Molecular formula structure of TIPA.

Triisopropanolamine (TIPA) was identified in the early nineties and used generally in the process of clinker grinding as a chemical grinder for lessening of agglomerates in the ball mill and to reform the particle distribution of the produced cement (Somasundaran and Shrotri 1995, Katsioti et al. 2009). The mechanical properties of cement are also improved by TIPA. Studies showed that the strength of OPC is greatly enhanced after 3 to 7 days when TIPA is added (Sandberg and Doncaster 2004, Huang and Shen 2011, Huang and Shen 2014). According to Gartner, Fe^{3+} and Al^{3+} which are the hydration products of ferrite, are chelated by TIPA, thereby promoting transport of ions. These chelated ions are then freed into the aqueous phase, as a result, building up ferrite dissolution and enhancing the complete silicate reaction (Gartner and Myers 1993). Another research on TIPA where 100 ppm amount of it was added in cement which was replaced with 10% (by

mass) limestone, showed an improved compressive strength of the cement especially on the 28th day, though also on the 7th day.

The methyl groups of TIPA are lipophilic in nature, thereby, enabling the release of gas into the cement mortar, leading to a decrease in the early stage compressive strength due to air-entraining effect (Sandberg and Doncaster 2004), although further addition of TIPA dosage would improve this effect. Also, upon further hydration, TIPA displays significant porosity decrease in the late period (Xu et al. 2017). The high efficiency of TIPA in the promotion of cement hydration has been reported by (Sandberg and Doncaster 2004), the reason for this could be attributed to the speed of formation of hydrated calcium sulphoaluminate and the formation of a complex TIPA-Fe due to the effectuated dissolution of ferric (Gartner and Myers 1993).

2.6 Applications of AAMs

The range of applicability of AAMs is wide, its use has been showcased in the following applications (Provis 2018);

- Plain and supplemented concrete production,
- Mortars, renders, and grouts production
- Precursor for the inactivation of organic and inorganic nuclear and toxic wastes
- Cemented reinforced and unreinforced concrete components and pipes
- Lightweight and foamed concretes

2.6.1 Advantages of AAMs

With regards to the proficiency of concrete and mortar, the effective use of slag in AAMs in their production has several advantages over OPC such as;

- Its hydration process releases lower heat (Arbi et al. 2016)
- Highly rich in calcium aluminosilicate content (Hajimohammadi et al. 2017)
- Lower CO_2 emissions (Collins and Sanjayan 2000, , McLellan et al. 2011, Yang et al. 2013)

- It has an early-stage development, hence, has higher mechanical strength (Chi 2016)
- Its refined pore structure enables it to have improved freeze-thaw resistance, strong resistance to fire, sulphate and acid attack (Rashad et al. 2012). The ability to resist chemical attack is one of the major advantages of AAMs over Portland cement, this has been established also for hydrochloric acid (Temuujin et al. 2011), sulphuric acid, nitric acid (Lloyd et al. 2012)
- Better resistance to chloride permeation (Roy et al. 2000)
- It enables high-value reaction pathway for aggregates (Provis 2014c)

The advantages of alkali-activated slags (AAS) outweighs that of OPC concrete, as it exhibits high and immediate strength development, it is also resistant to chemical attack (Wang and Scrivener 1995). Moseson et al. 2012, calculated 97% savings of CO_2 and energy when Na_2CO_3 is used to activate a granular limestone content BFS mortar.

However, processing and application of AAMs in construction are currently faced with difficulty related to sourcing and ensuring increase in the availability of a competent co-binder that would enable control over the deformation and flow behaviour of the geopolymer paste. Earlier attempt to curb this challenge brought about the use of organic compounds which contributed to an improved performance of the activated materials (Marchon et al. 2013, Kashani, Provis, Xu, et al. 2014), thought the degree of rheology it offered was below that attained using superplasticizers in OPC concrete (Provis 2018). However, characterization of the liquid-solid interface in alkali-activated mortars is considered a more crucial factor for enhancing performance (Kashani, Provis, Qiao, et al. 2014).

3 Materials and experimental methods

3.1 Geopolymer starting materials, preparation and mix design

This chapter addresses the steps, methods and techniques used in this research, it explains also the analytical procedures, sizes of sample materials, and the entire executed research plan for achieving the stated aim and objectives.

The starting materials used in the preparation of the geopolymer matrix were Blast furnace slag supplied by Finnsementti Oy (Fig.7a), Stonewool waste from Paroc Oy (Fig. 7b), Desulphurization dust, a waste material supplied by SSAB steel work (Fig. 7c), all from Finland. These materials are sources of calcium aluminosilicates in the AAM synthesis. Other materials used includes, standard sand (EN 196-1) with grain size between 0.08-2.00 mm which were evenly distributed using a spinning riffler Fig. 8, demineralised water and TIPA. The chemical compositions of these raw materials were determined with X-ray fluorescence (XRF) spectroscopy, the result is shown in Table 1 below.

Figure 7. (a) BFS, (b) SW before milling, (c) De-dust.

Figure 8. Spinning riffler used to divide the sand equally

3.1.1 Milling of stonewool waste

A Germatec ball milling machine as shown in Fig. 9a, was used in milling the stonewool waste to 10µm shown in Fig. 9b. A total of 100 steel balls of different diameters: 25mm, 30mm and 40mm were placed at different angles in a 10 litre ball container containing also the stonewool waste. For each round of mill, 500 grams of stonewool was milled for 4 hours at 263 rpm. The functionality of these equipment and the desired particle size result depends on the number of balls, their different sizes, speed of the milling machine, and the duration.

(a) (b)

Figure 9. (a) Germatec ball milling; (b) Milled stonewool waste

Table 1. Chemical Composition (CC) Of Blast Furnace Slag, Stonewool, and De-sulphurization dust as determined by XRF

Chemical Compositions (%)	**Desulphurization dust**	**SW**	**BFS**
Na_2O	28.8	1.4	0.5
MgO	0.4	11.2	10.2
Al_2O_3	0.3	16.3	9.5
SiO_2	2.4	40.4	32.3
P_2O_5	0.03	0.1	0.01
SO_3	5.1	0.1	4.0
K_2O	1.4	0.6	0.5
CaO	35.7	17.9	38.5
TiO_2	0.18	1.0	2.2
Fe_2O_3	14.8	8.8	1.23

3.1.2 Particle size distribution analysis

Particle size distribution analysis of BFS, SW and De-dust were carried out using Beckman Coulter LS 13320 laser diffraction particle size analyzer, shown in Fig 10. For each sample, 0.3 g was used. A 100 ml isopropanol was also measured in a glass beaker, from where a small amount was used to first dissolve the sample in a flat glass crucible, before adding the mixture into the glass beaker and stir. This was then placed in the ultrasonic bath for two minutes to aid in further dispersion of the particles, after which it was added into the machine at a minimum of 8% and maximum of 12%, before starting the analysis.

Figure 10. Beckman Coutter LS 13320 laser diffraction particle size analyzer

3.1.3 Matrix Preparation

Materials for the first step of mixing of mortar samples, were measured according to Table 2, showing the 16 different mix compositions. The BFS, SW and De-dust were first added to a Kenwood mixer and mixed together at medium speed for 1 minute to obtain a dry homogenous mixture. 180g of demineralised water was added, and then the speed was increased a little above medium and mixed for one minute, after which the underneath and walls of the mixer was scraped for 30 seconds to ensure that all samples were mixed. The mixing continued for another 3 minutes at a high speed, after which 800 g of standard sand was added and mixed for one more minute. After this, the paste was manually stirred before placing it on the spread test machine. All the various mix compositions were prepared using the same sand-to-binder mass weight ratio (s/b), and a constant water-to-binder weight ratio (w/b). Starting from mix 5 to 16, TIPA was added to the 180 ml of water and was shaken to enable the TIPA dissolve properly, before adding to the mixture in the Kenwood mixer. The TIPA amount was increased (0.05%, 0.1%, 0.15% and 0.20%) in the mix based of the De-D and stone wool weight percentage.

Table 2. 16 Mix Proportions for the Mortar Samples (in grams). Where, a=0.05%TIPA, b= 0.1% TIPA, c = 0.15% TIPA

Sample (g)	0% SW	5% SW	10% SW	15% SW	0% SWa	5% SWa	10% SWa	15% SWa
Stonewool	0	20	40	60	0	20	40	60
Des-dust	80	80	80	80	80	80	80	80
BFS	320	300	280	260	320	300	280	260
Demin-water	180	180	180	180	180	180	180	180
TIPA	0	0	0	0	0.04	0.05	0.06	0.07
Sand	800	800	800	800	800	800	800	800
Sample	0% SWb	5% SWb	10% SWb	15% SWb	0% SWc	5% SWc	10% SWb	15% SWc
Stonewool	0	20	40	60	0	20	40	60
Des-dust	80	80	80	80	80	80	80	80
BFS	320	300	280	260	320	300	280	260
Demin-water	180	180	180	180	180	180	180	180
TIPA	0.08	0.1	0.12	0.14	0.16	0.2	0.24	0.28
Sand	800	800	800	800	800	800	800	800

3.2 **Spread-flow Test**

Spread-flow test was performed on the fresh paste so as to evaluate the workability by measuring flowability of the paste according to ASTM standard C1437. The fresh paste was let into a two layer right circular conical cone mould placed on a flat glassy plate of the machine in Fig. 11 below. Both layers are compacted by at least 10 strikes with a stick. After the mass was compacted and the top surface leveled, the cone was vertically removed, giving way for the paste to flow. The flow table handle was then turned 15 times within 15 seconds, in a circular-like movement, then two perpendicular directions of the spread paste was immediately measured and averaged. The spread-flow percentage was calculated using the formula below;

$$\frac{d - d_0}{d_0} \times 100 \qquad (5)$$

Where, d = average of the measured diameters of the spread paste

d_0 = bottom diameter of the circular conical coned which was measured at 100mm

After the spread-flow test, the fresh pastes were cast into a 20 x 20 x 20 mm rectangular moulds as seen in Fig. 12a and 12b, and were placed on a jolting table to compact the paste according to EN 196-1, and to remove air bubbles. The moulds were each sealed in a plastic bag to avoid water loss caused by evaporation during curing (Fig. 12b). All the mixture samples were cured at 60ºC and demolded after 24 hours. The samples were placed in a 22ºC humidity chamber at about 50% relative humidity until 7days and 28days strength tests and further analysis.

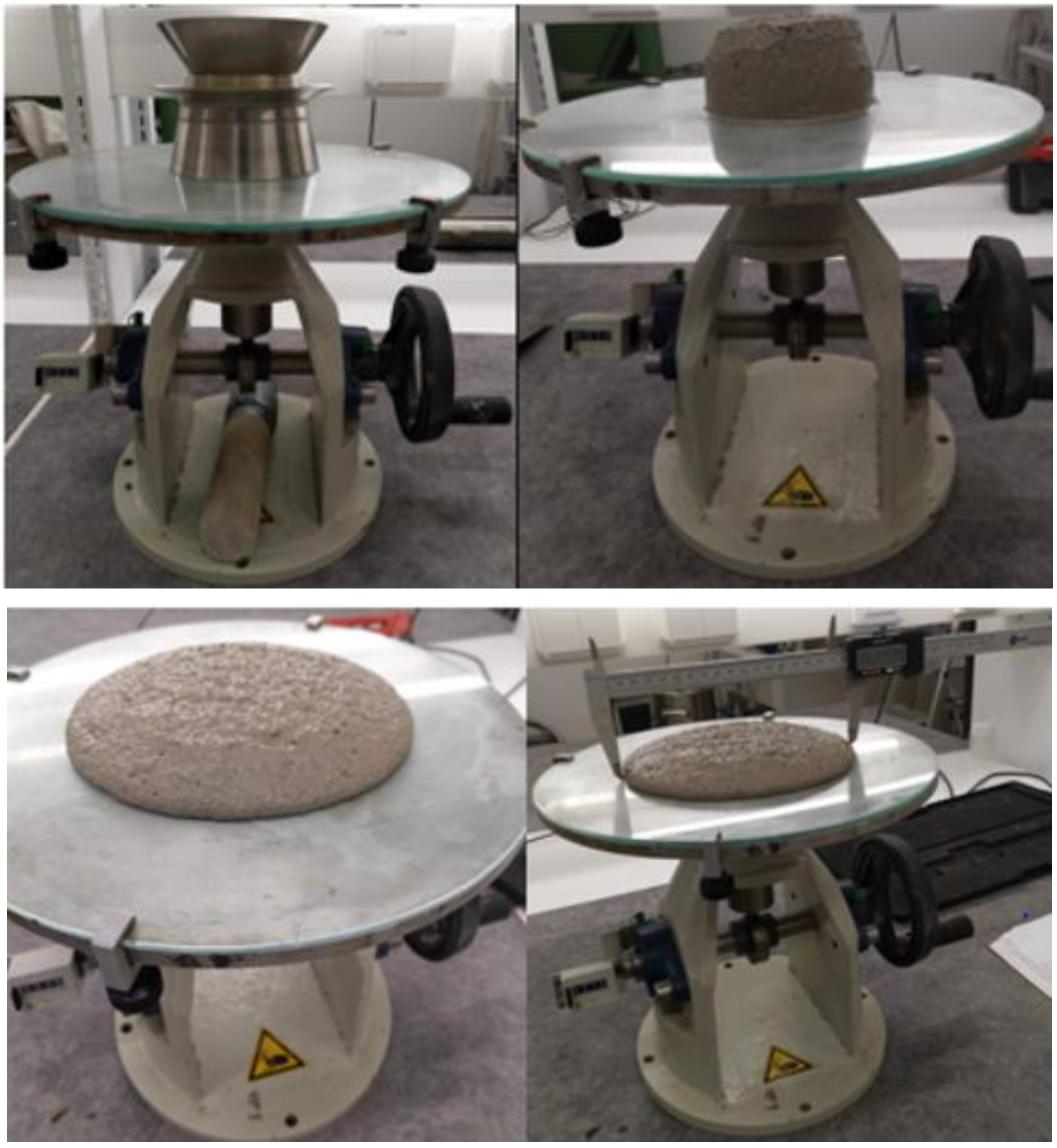

Figure 11. Pictorial view of Spread-flow Test.

(a)

(b)

Figure 12. (a) 20 x 20 x 20 mm casting mould; (b) sealed 20 x 20 x 20 mm casting mould.

3.2.1 Setting time test

The same mix proportions in table 2 above was used in preparing samples for the setting time test, though standard sand was excluded in the mixture. According to ASTM C191-08, a Vicatronic Matest setting time machine was used for this test. The machine was first set up by calibrating the cylindrical 40 mm mould, and setting the time interval for penetration of the pin for every 5 minutes. Then the time for adding water to the measured precursors, and time for starting the experiment were also set for each of the 16 mixes.

The precursors were measured in a plastic beaker, 100ml of demineralised water was added to it at the specified time, then using a high shear mixer to mix the samples for 5 minutes. The mixture was poured in the 40mm cylindrical mould and placed on a vibrating disk for 30 seconds, to ensure it is properly settled. The mould was placed on the flat section of the Vicatronic machine (Fig.13) before the fixed starting time when the needle will first penetrate through the paste and down to the bottom of the 40mm calibrated mould height. The same procedure was repeated for the 16 mix proportions, although from mix 5, different amounts of TIPA was added to the 100g of water and was shaken to dissolve before adding the water to the sample.

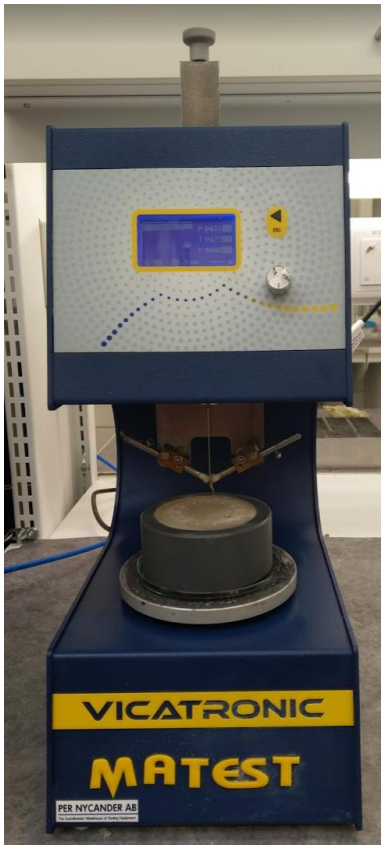

Figure 13. Equipment for Setting Time.

3.3 Characterization methods

3.4 Strength tests

Two samples from each of the 16 mix compositions were used to measure the flexural and compressive strength of the mortars. The surface of the mortars was smoothened with

a sand paper to enable a balance impact during the test. These tests were carried out on the 7 and 28 days after curing, using Zwick Z100 material testing machine.

3.4.1 Flexural strength test

Over a supported span of 40mm, flexural load was applied on the centre point of each mortar with a maximum load capacity of 100KN and a speed of 0.05 K/N, using a three-point bending test mode as shown in Fig.14. Results were obtained using equation 6, according to SFS-EN 196-1.

$$\sigma F = \frac{3FD}{2bx^2} \quad (6)$$

Where,

σF = flexural strength in MPa

F = maximum load at breaking point, in N

d = support span length, in mm

b = width of sample mortar, in mm

x = thickness of the sample, in mm

Figure 14. Three-point bending test mode for flexural strength test.

3.4.2 Compressive strength test

Compressive strength of the mortars was measured under a compressive load with maximum capacity of 100kN using a compressive speed of 2.4kN/s. Fig. 15 shows the set up as used in the test. Equation 2 below was used in calculating the compressive strength.

$$\sigma c = \frac{F}{A} \quad (7)$$

Where

σc = compressive strength, in MPa

F = maximum load at crush point, in N

A = surface area of the mortar on which the load is asserted, in mm^2

Figure 15. Compressive strength test

3.5 Solvent exchange

Acetone was used to stop particles reaction in the paste samples, so as to enable the use of the samples for further analysis such as the microstructural analysis. The same mix

proportions and preparation procedure as was used in the setting time paste, was also employed for this test. In this case, the paste was poured and covered in a 10 ml plastic container, and kept under room temperature. After 7 and 28 days respectively, each sample was grinded to fine powder and was added to another plastic container, then acetone was added such that it covered the sample, and was allowed to dry for about 36 hours, after which the container was placed in a dessicator until the microstructural analysis.

3.5.1 Dissolution test

Dissolution/solubility tests in alkaline solution enables a straight detection of the amount of reactive species of silicates and aluminates present in the staring raw materials. This test was carried out to determine the dissolution ability of the chemical compositions of the starting raw materials used in this work. Mixture samples with 5% SW was used for this test. The 0.1g of each sample mixtures were as described in Table 3 below, 40ml of 6M NaOH solution was added to each sample in polypropylene bottles and were placed for 24 hours under shaking motion at a speed 200/min using a horizontal shaking table (IKA KS 260 orbital shaker) shown in Fig. 16. Each mix was then filtered using 0.45 μm polypropylene filter paper, each of the filtrate was acidified with HNO_3 to pH below 2, after which all mixes were analysed for the presence of Ca, Si, Al and Fe using inductively coupled plasma atomic emission spectroscopy (ICP-OES).

Table 3. Solubility text sample mixtures.

Materials (grams)	5% SW	5% SWa	5% SWb	5% SWc
SW	0.06	0.06	0.06	0.06
BFS	0.2	0.2	0.2	0.2
De-Dust	0.76	0.76	0.76	0.76
TIPA	0.00	0.0005	0.001	0.0015

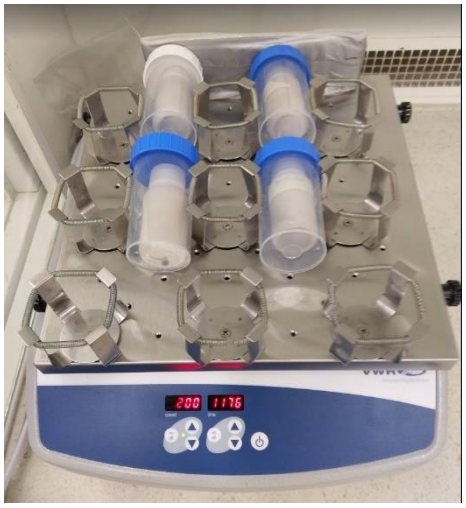

Figure 16. Horizontal shaking table (IKA KS 260 orbital shaker).

3.5.2 Thermogravimetric (TGA) analysis

Thermogravimetric (TGA) analysis was carried out on the 16 solvent exchanged samples after 28 days. It was done using Precisa PrepASH 129 analyzer. The weight of each sample was measured below 3.5g and was placed in alumina crucible, all were analysed at a temperature range from ambient up to 1000^{o}C

3.5.3 X-ray diffraction (XRD) analysis

To identify the crystalline phases of the alkali activated material, XRD analysis was carried out on 5% SW solvent exchanged geopolymer samples after 7- and 28-days aging, using a Siemens D500 x-ray powder diffractometer. The machine (Siemens AG, Germany) was configured with Cu-Kα radiation which was utilised in the collection of the diffraction patterns. For each sample, 0.27g was mixed with 0.3g of TIPA and were ground to fine powder before use.

3.5.4 Iso-thermal calorimetry

Calorimetric analysis of the precursors was carried out using 5% SW sample mixtures to determine the heat evolution of the precursors in the geopolymer matrix, this was observed using Isothermal Conduction Calorimeter (TAM AIR, TA INSTRUMENTS INC)

at ambient temperature for 7 days. The observed cumulative heat during the geopolymerization reaction was measured by linking its heat flow with time, which lasted for 90 hours.

3.5.5 Efflorescence assessment

Efflorescence was observed to determine the effect of alkaline or soluble silicates which were not completely consumed during the geopolymerization synthesis. Efflorescence takes place when alkaline ions from pore solution are transferred to the surface of the sample(s) and then react with atmospheric CO_2. Two samples from each of the 16 mixes were subjected to efflorescence tests 21 days after curing.

4 Results and discussions

The experimental procedures designed for this work was to evaluate the use of an alternative alkali activator for SW and BFS. The amount of SW used for each sample analysis showed much significant effect on the results, hence the result of these procedures has been grouped based on the percentage of SW used which are; 0% SW, 5% SW, 10% SW and 15% SW, amount of TIPA, and the molar ratio of the chemical contents of the precursors as shown in table 4. The mix composition assumes complete dissolution of the binders. However, it should be noted that the overall molar ratios do not necessarily account for the complete dissolution of the solid precursors, hence it should not be regarded as being the representative dissolution of the binder gel; the molar ratios are used for mix design purposes only.

Table 4. Calculated molar ratios in the binder composition.

Samples	SiO_2/CaO (mol)	SiO_2/Al_2O_3 (mol)	Na_2O/ Al_2O_3 (mol)	Na_2O/Si (mol)
0SW	0.64	5.77	1.08	0.19
5SW	0.67	5.61	1.04	0.19
10SW	0.70	5.47	1.01	0.18
15SW	0.73	5.34	0.98	0.18

4.1 Properties and microstructure of precursors.

The properties and microstructure of the geopolymer precursors was determined by analysing their particle size distribution, quantitative x-ray diffraction (QXRD), thermogravimetry and differential analysis (TGA/DTG).

4.1.1 Particle size distribution (PSD) of precursors

Reactivity of geopolymer precursors can be affected by the particle size distribution of the raw materials. A smaller sized PSD gives rise to effective alkali-activation reactions, and thus enhances the final mechanical properties (Assi et al. 2018). Fig. 17 showed the

PSD of SW, BFS and de-dust with median size particle diameters of 8.6µm, 12.9µm and 3.3µm respectively. The sizes are considered appropriate for effective rheology of the geopolymer paste. The median value recorded for SW showed that the three hours ball milling was sufficient enough to yield fine particles for the geopolymer matrix.

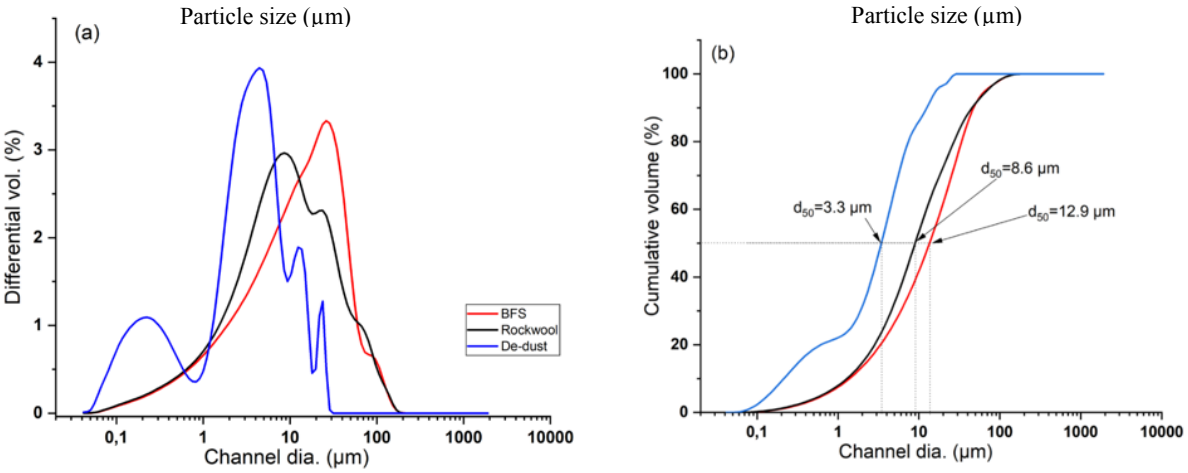

Figure 17. Particle size distribution and median size of SW, FBS and de-dust.

4.1.2 Spread-flow test

The workability of the geopolymer mix as determined by the spread-flow test showed an average flow diameter range between 158 mm to 196 mm. The percentage of SW and TIPA was observed to have significant effect on the flow of the paste as seen in Table 6. The average diameter range of the geopolymer paste showed that the geopolymer have both high and moderate workability according to the criteria given by (Ghosh and Ghosh 2012).

4.1.3 Effect of Si/Ca, Na/Al, Si/Al and TIPA on workability and setting time

At 0% SW, 76.3% flowability was recorded which increased with 16.3% when 0.05% TIPA was added. The lowest flow percent at 57.9% was also recorded even with further increase in TIPA which had no influence. This is because samples with 0% SW had the highest amount of Si/Al molar ratio (5.77) and Na/Al molar ratio (1.08). These Increase

in the dosage of soluble silicate and alkali content raises the viscosity of geopolymer matrix resulting in the reduction of the flow diameter (Ghosh and Ghosh 2012).

When 5% SW was added, flowability reduced with 2.2% but increased with 5.1% with the addition of 0.05% TIPA. The highest flow percent was recorded at 96.2% when 0.1% TIPA was added to 5% SW samples with 0.67, 5.61 and 1.04 molar ratios of SiO_2/CaO, SiO_2/Al_2O_3, and Na_2O/Al_2O_3 respectively**.** This can be attributed to the solubility of the chemical content of the SW (Kinnunen et al. 2017), that was greatly enhanced by addition of TIPA which according to (Huang and Shen 2011) is classified as quality improver, and promotes effective homogenization of the elements of cement such as BFS, gypsum and clinker (Allahverdi et al. 2018), when added moderately.

Generally, for 0% SW samples, addition of 0.05% TIPA increased their flowability to 80%. And for samples with 5% SW, lower flowability compared to 0%SW samples was observed, however, the flowability accelerated greatly when 0.1%TIPA was added. Samples with 10% and 15% SW recorded lower followability compared to 5% SW samples. Addition of 10SW and 15SW resulted to 13.3% and 3.3% decrease in flowability respectively. The reduced flowability in 10% and 15% SW samples is attributed to the increased amount of the fibrous content of SW, causing difficulty in flowability of the samples.

The trend in flowability from 0% SW to 15% SW showed that addition of SW can reduce flowability but can be increased with the addition of TIPA. However, addition of TIPA becomes less significant when higher amount of SW is added. Fig. 18a, b, c, and d shows the graphical view of this trend. Based on the average diameter of the flow, the workability of the geopolymer mixes can be classified according to the criteria in Table 5 below (Ghosh and Ghosh 2012).

Table 5. Ghosh and Ghosh Criteria for determining the workability of geopolymer mix

No	**Flow Diameter**	**Workability**
1	Above 250	Very High
2	180 to 250 mm	High
3	150 to 180 mm	Moderate
4	150 to 120 mm	Stiff
5	Below 120 mm	Very stiff

Table 6. Observed setting time and spread-flow percentage

	0% SW	**0% SWa**	**0% SWb**	**0% SWc**	
Initial Setting Time (Minutes)	207	104	97	159	
Final Setting Time (Minutes)	317	344	325	354	
Spread (%)	76,3	80,0	68,5	57,9	**0% SW**
	5% SW	**5% SWa**	**5% SWb**	**5% SWc**	
Initial Setting Time (Minutes)	215	210	149	181	
Final Setting Time (Minutes)	350	346	281	397	
Spread (%)	74,1	79,2	96,2	81,1	**5% SW**
	10% SW	**10% SWa**	**10% SWb**	**10% SWc**	
Initial Setting Time (Minutes)	183	111	194	187	
Final Setting Time (Minutes)	308	196	326	493	
Spread (%)	63	77,2	69,6	76,5	**10% SW**
	15% SW	**15% SWa**	**15% SWb**	**15% SWc**	
Initial Setting Time (Minutes)	232	213	246	192	
Final Setting Time (Minutes)	348	393	431	480	
Spread (%)	72,7	69	71,9	73,5	**15% SW**

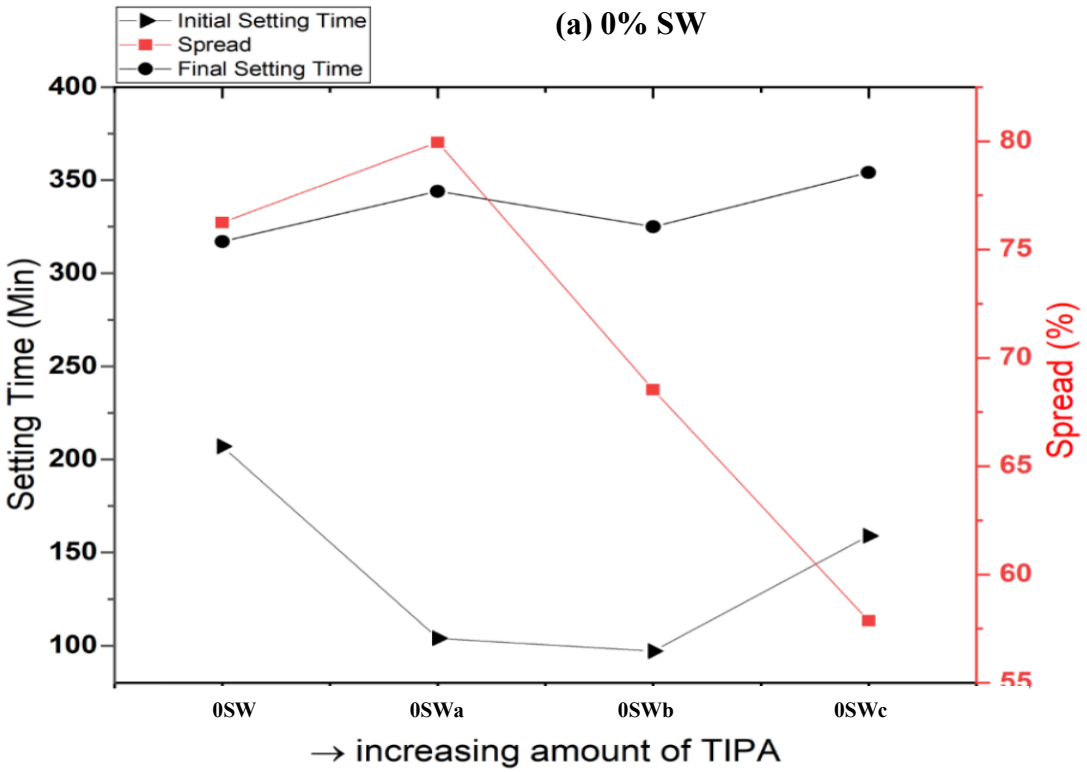
(a) 0% SW
Initial Setting Time
Spread
Final Setting Time
Setting Time (Min)
Spread (%)
400
350
300
250
200
150
100
80
75
70
65
60
55
0SW
0SWa
0SWb
0SWc
→ increasing amount of TIPA

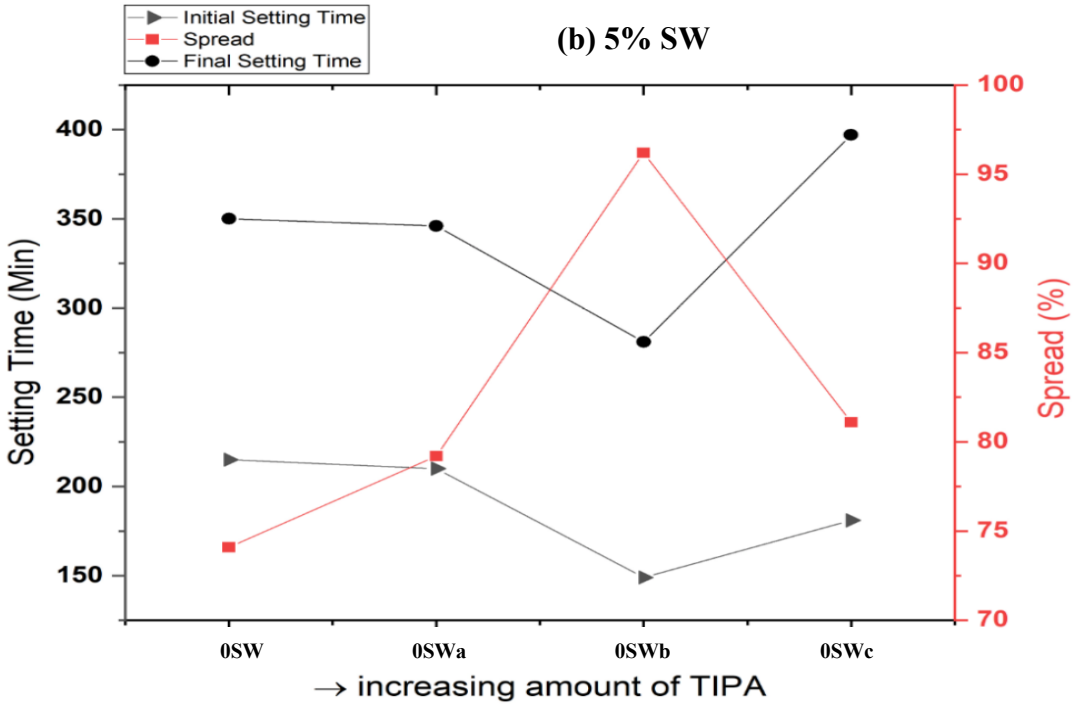
(b) 5% SW
Initial Setting Time
Spread
Final Setting Time
Setting Time (Min)
Spread (%)
400
350
300
250
200
150
100
95
90
85
80
75
70
0SW
0SWa
0SWb
0SWc
→ increasing amount of TIPA

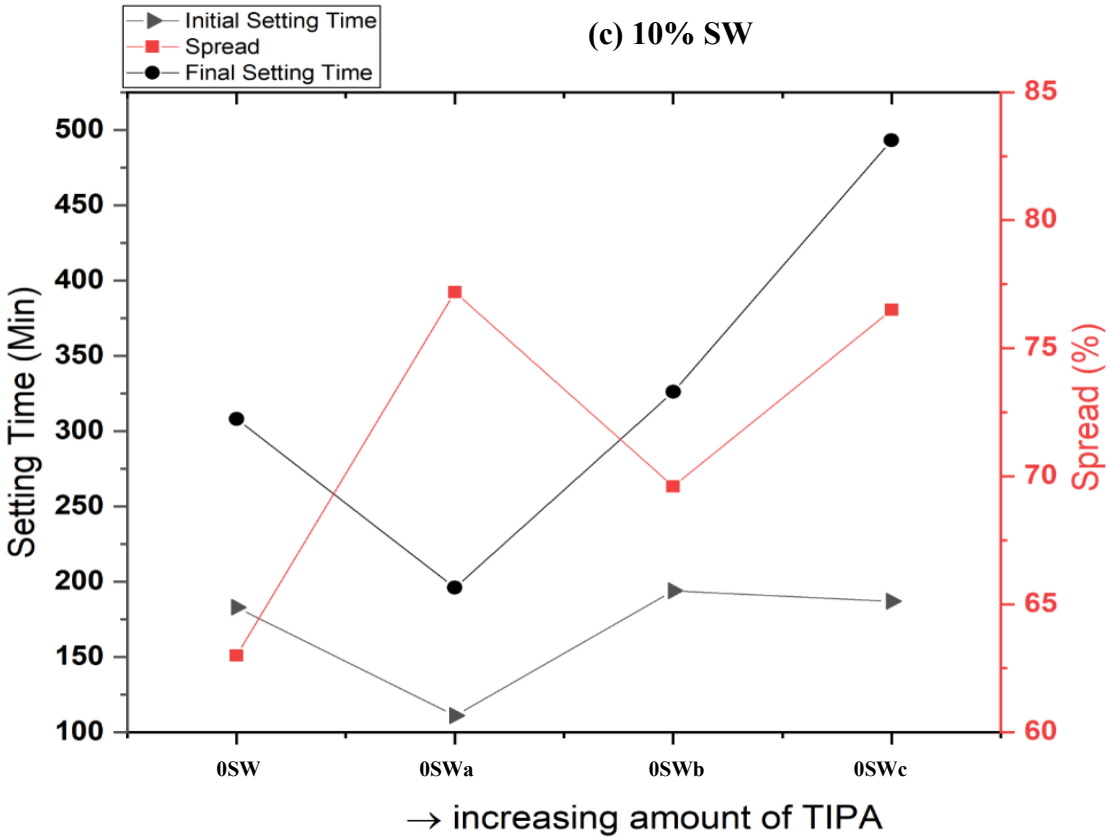
(c) 10% SW
Initial Setting Time
Spread
Final Setting Time
Setting Time (Min)
Spread (%)
500
450
400
350
300
250
200
150
100
85
80
75
70
65
60
0SW
0SWa
0SWb
0SWc
→ increasing amount of TIPA

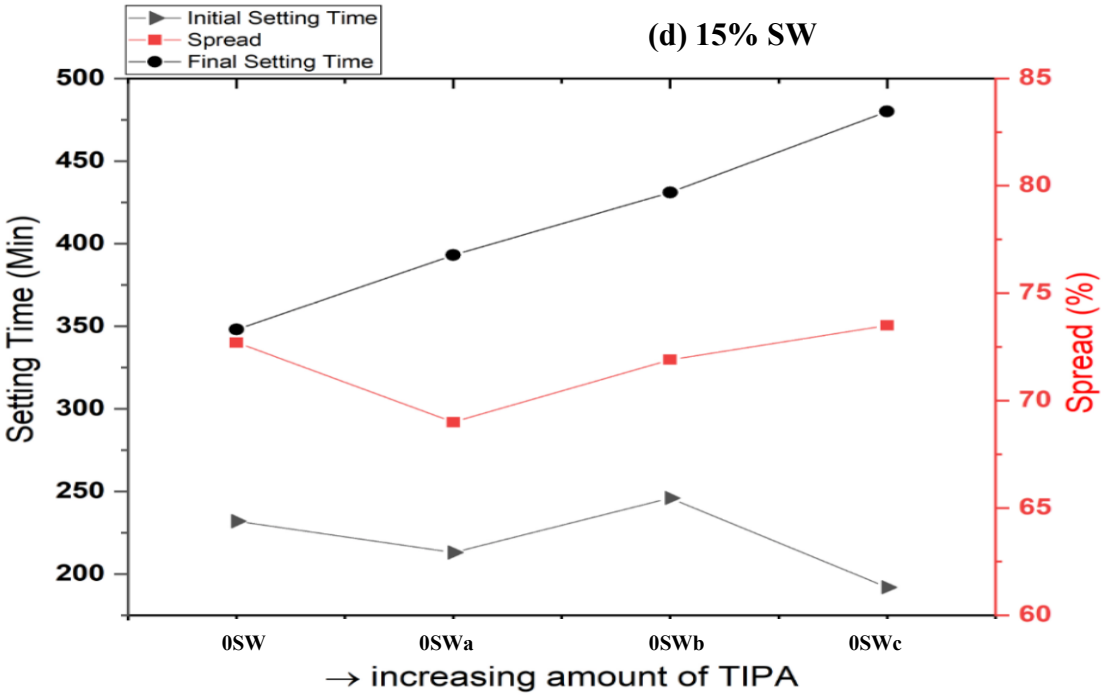

Figure 18. Graphical view of setting time and workability of pastes for (a) 0% SW (b) 5% SW (c) 10% SW, and (d) 15% SW

The setting time recorded from the test samples varied between 97-246 minutes for the initial setting time, while the final ranged within 196-493 minutes as shown in Table 6. Initial setting time for all samples with 0.05% TIPA was lower than the initial time for samples without TIPA. This is presumably because of the aid offered by TIPA for the dissolution of the precursors´ chemical contents. Addition of 0.1% TIPA to 0% SW samples recorded the lowest initial setting time of 97 minutes which could be attributed to the absence of SW, and addition of the TIPA which accelerated the dissolution thereby shortening the setting time.

The final setting time for samples with 15% SW had the most consistent high setting time range between 348-480 minutes, while 10% SW sample with 0.15% TIPA recorded the highest final setting time at 493 minutes. These ranges are graphically shown in Fig. 18 above. These higher setting times observed in 10% and 15% SW samples despite the increased amount of TIPA, is associated with the physical structure of SW which contains thick fibres between 5 µm to 10 µm (Kinnunen et al. 2017), resulting in reduced rate of dissolution, hence lengthening the setting time. Higher amount of SW is therefore said to cause longer setting time due to its thick fibre content.

4.2 Mechanical strength

Mechanical strength of the formed geopolymers was reported with the compressive and flexural strength as shown in figure 19 and figure 20 respectively.

4.2.1 Compressive strength

The highest compressive strengths of 16.6 MPa and 20.1 MPa was observed from 5% SW samples having 0.05% TIPA at 7 and 28 days respectively as shown in Fig. 19a, b, c and d. This could be attributed to the solubility of the silicon and aluminium content of SW (Kinnunen et al. 2017), and also with the aid of TIPA which according to (Huang and Shen 2011) is classified as quality improver, and promotes effective homogenization of the elements of cement such as BFS, gypsum and clinker (Allahverdi et al. 2018), when added moderately

The lowest compressive strength of 12.3 MPa was recorded at 7 days in samples with 10% SW without TIPA. Further decrease in strength was noticed with increase in SW content. This shows that higher amount of SW could result to partial or incomplete dissolution due to difficulty in mixing the thick fibre content of the high SW amount. Similar result was achieved in the production of geopolymer using mineral wool and metakaolin (Adesanya, 2015).

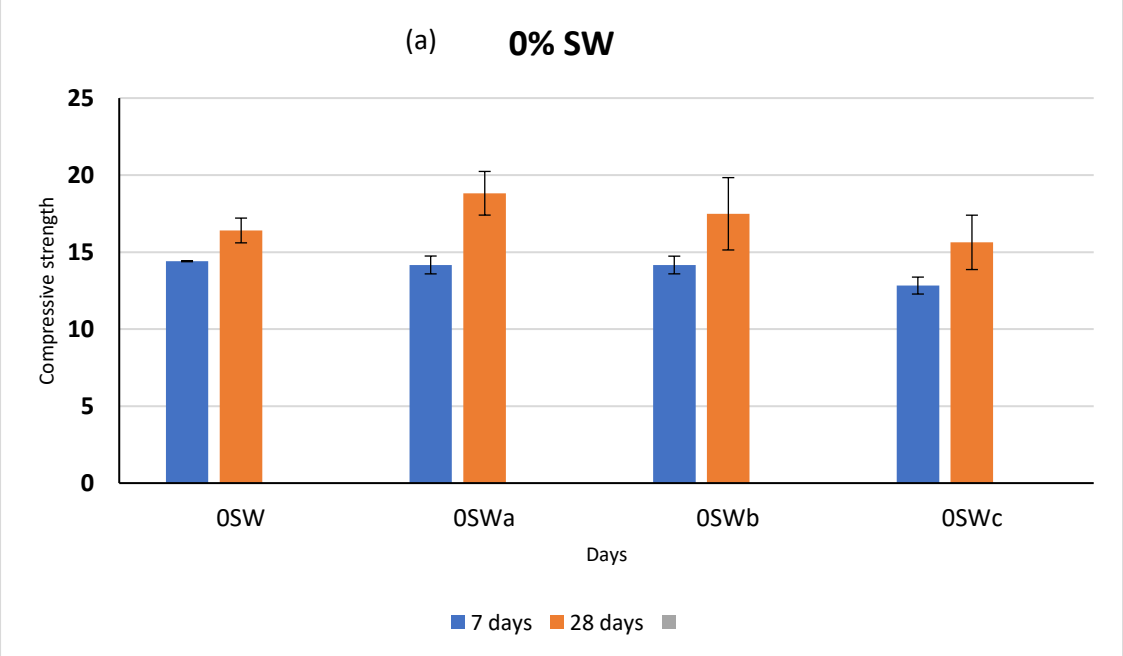

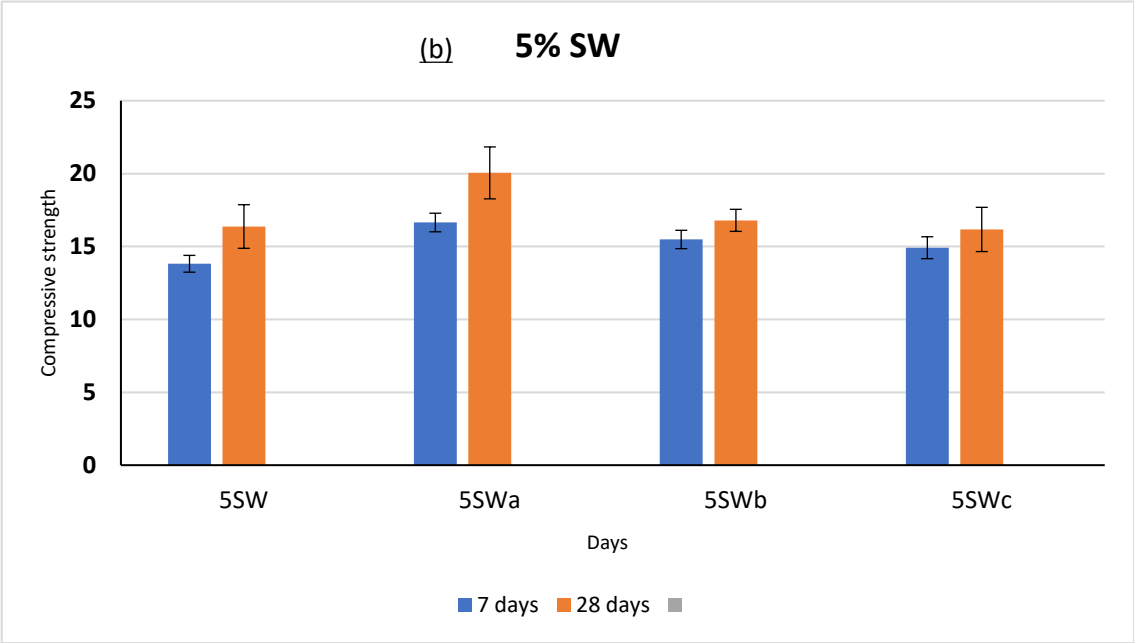
(b) 5% SW
25
20
15
10
5
0
Compressive strength
5SW
5SWa
5SWb
5SWc
Days
7 days
28 days

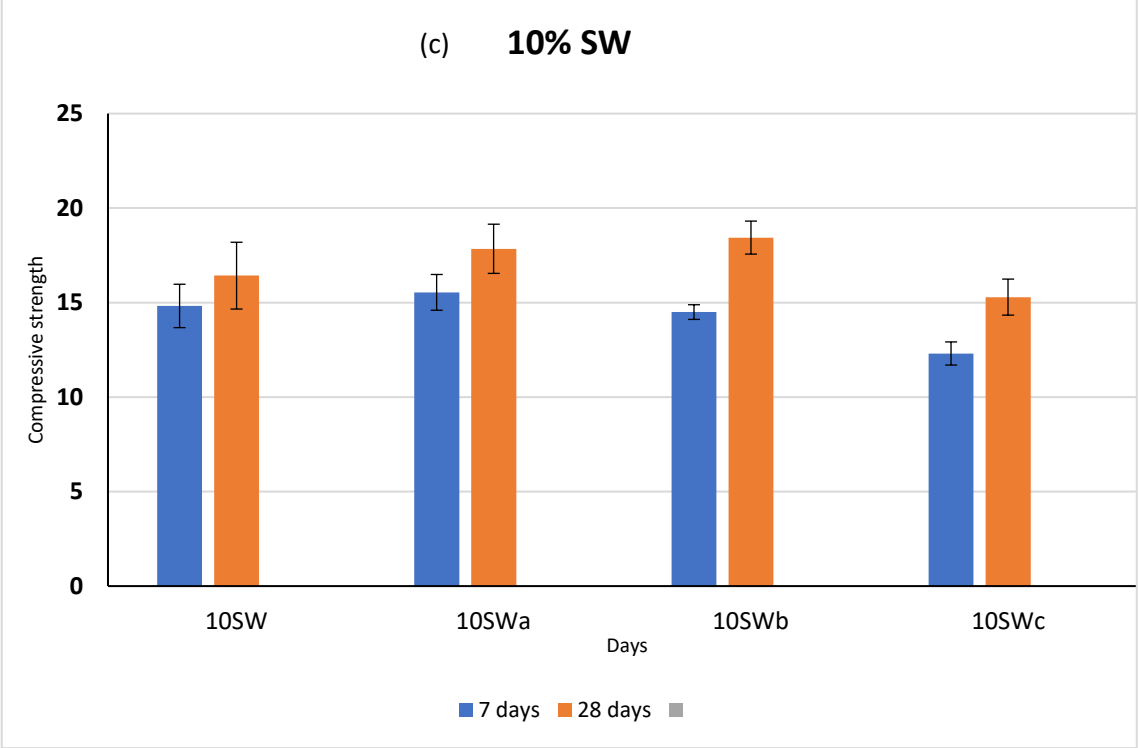
(c) 10% SW
25
20
15
10
5
0
Compressive strength
10SW
10SWa
10SWb
10SWc
Days
7 days
28 days

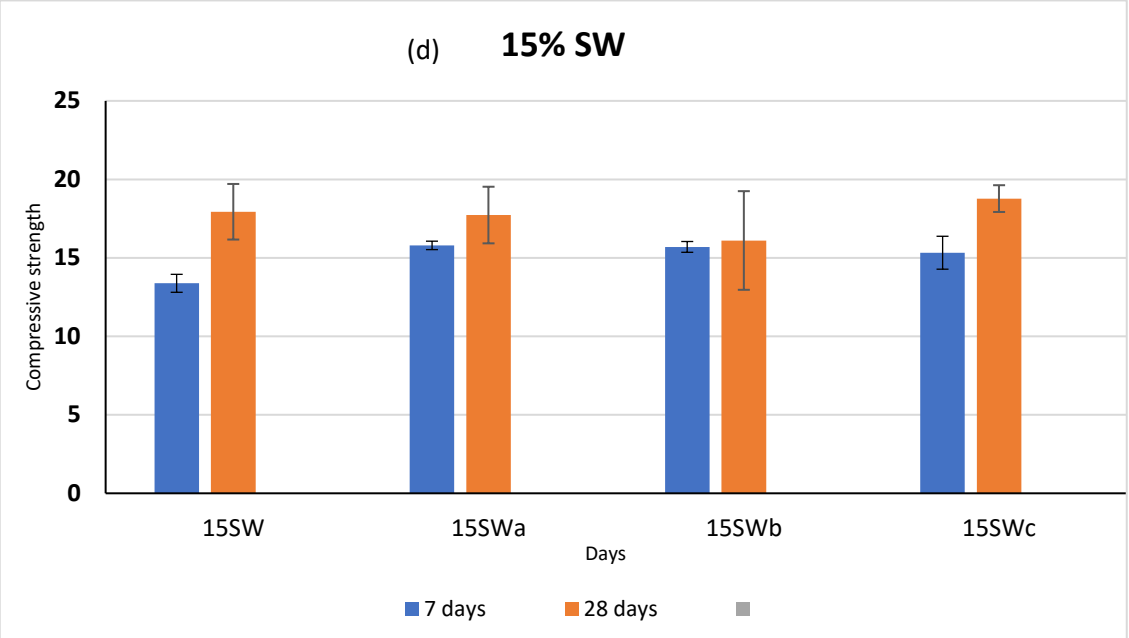

Figure 19. Compressive strength chart for (a) 0% SW (b) 5% SW (c) 10% SW, and (d) 15% SW

4.2.2 Flexural strength

The highest flexural strength of 5.9 MPa shown in Fig. 20a, b, c and d, was measured at 28 days, in samples with 0% SW, but higher amount of BFS and 0.1%TIPA, this could be credited to the effect of TIPA, and also BFS which reforms the reaction products and pore structure in thickened concrete, thus, enhancing the flexural strength mainly at the further ages (Özbay et al. 2016).

Flexural strength measured the lowest strength of 3.5 MPa at 7 days in samples with 5% SW and 0.15% TIPA. This is because flexural strengths is exceptionally responsive to micro-cracks (Özbay et al. 2016), therefore micro-cracks present inside the samples could be associated to the reason for the low flexural strength (Hubler et al. 2011, Thomas et al. 2012, Ye and Radlińska 2017).

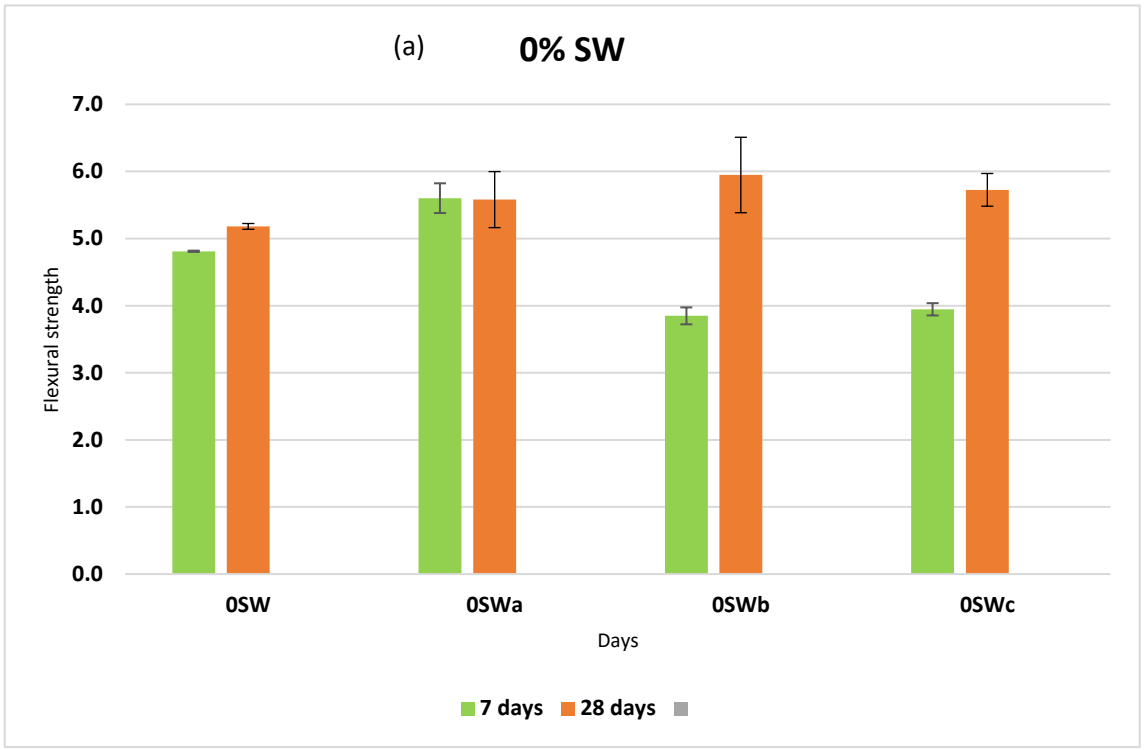
(a)
0% SW
7.0
6.0
5.0
4.0
3.0
2.0
1.0
0.0
Flexural strength
0SW
0SWa
0SWb
0SWc
Days
7 days
28 days


(b)
5% SW
6.0
5.0
4.0
3.0
2.0
1.0
0.0
Flexural strength
5SW
5SWa
5SWb
5SWc
Days
7 days
28 days

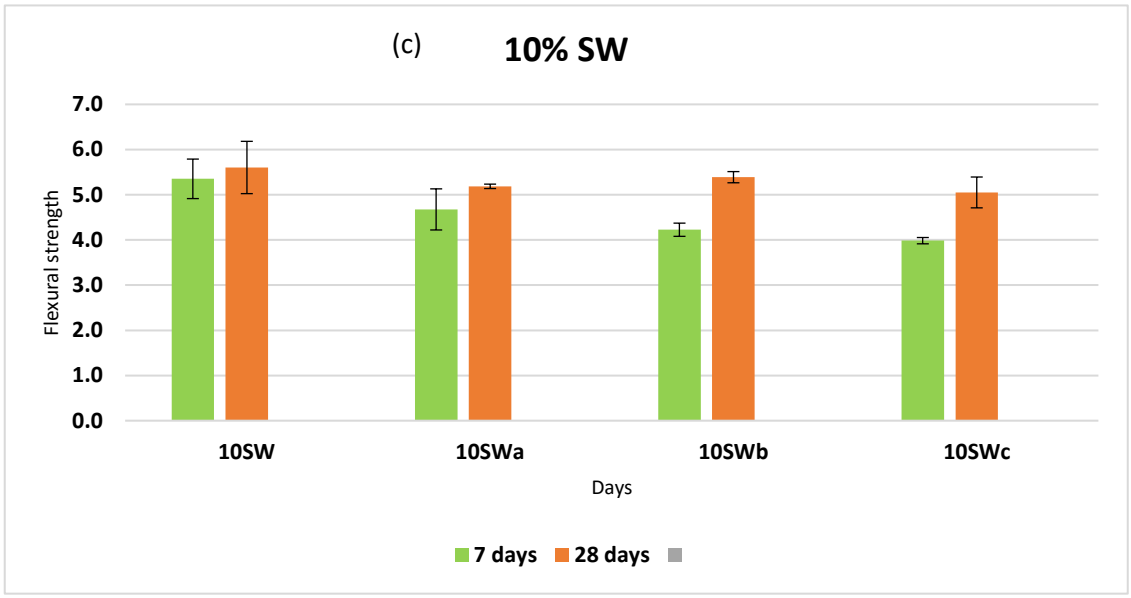

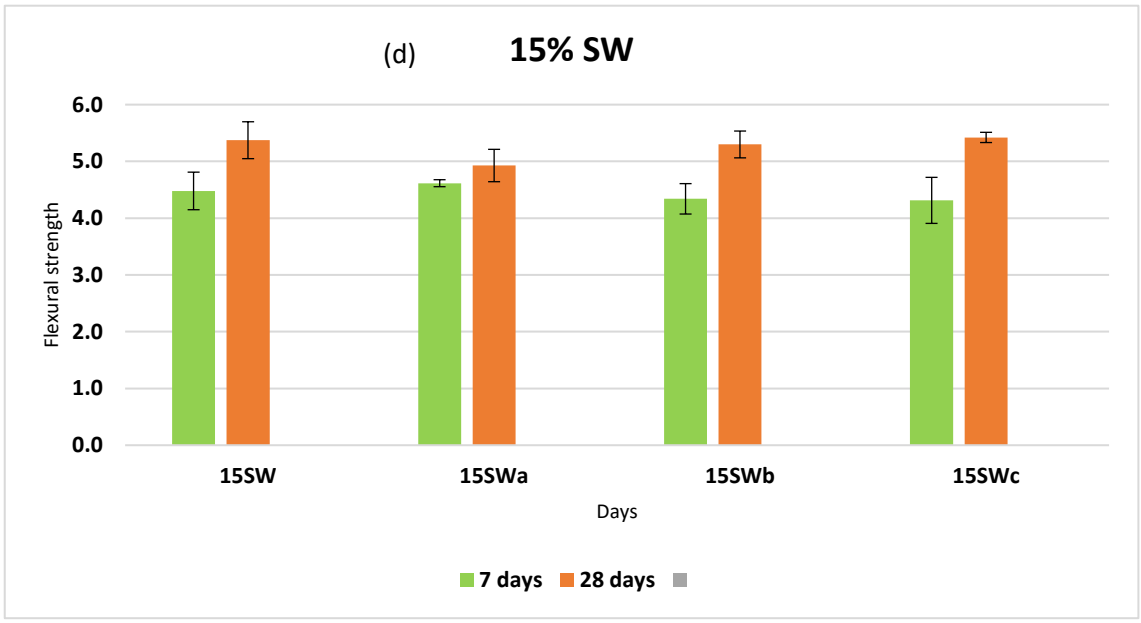

Figure 20. Flexural strength chart for (a) 0% SW (b) 5% SW (c) 10% SW, and (d) 15% SW

4.2.3 Effect of Si/Ca, Na/Al, Si/Al and TIPA on strength

The lowest compressive strength measured in samples with 10% SW samples could be attributed to minimal activator content in Na_2O/Al_2O_3 leading to insufficient alkali required to initiate geopolymerization process. It can be explained also that the fibre content in the 10 % SW samples was too high to be dissolved by the lesser alkali content in the mixtures.

Optimum molar ratios of Na_2O/Al_2O_3, SiO_2/CaO and SiO_2/Al_2O_3 were 1.04, 0.67 and 5.61 respectively in 5% SW samples, from where highest compressive strength was observed. This showed that the mixture contains sufficient alkali, silicon and aluminum content for effective geopolymerization, hence increasing the strength. It has been reported that high alkaline solution up to certain limit increases mechanical strength (Nath and Sarker 2014, Humad et al. 2018).

The high amount of SiO_2/CaO and SiO_2/Al_2O_3 ratios present in 5% SW also contributed to the high strength of the samples because the formation of sodium silicate as a result of the high Na and Si content, promotes the compressive strength of BFS-based geopolymer samples by improving the rate of dissolution of silicon and aluminum, where Al-O bonds dissolves rapidly in the high alkali environment as it has weaker bonds than the Si-O bonds (Fernández Carrasco et al. 2007, Mohammed et al. 2019) contained in the raw material. Therefore, the availability of silicon ion in the original raw material(s) prior its provision during the dissolution reaction could increase the rate of geopolymerization reaction thereby promoting the strength (Nadoushan and Ramezanianpour 2016).

Higher amount of CaO contained in the de-dust, can yield hydroxyl ions in the presence of water which increases the pH of the solution, thereby triggering the hydration of BFS for the geopolymerization reaction and thus, promoting the strength, also, the formation of carbonates of sodium and calcium in dry activators could pose as filler material, thus, reducing the pore sizes of the paste leading to lesser water absorption and consequently increase the compressive strength (Abdel-Gawwad and Abo-El-Enein 2016). Also, geopolymerization can be further increased by obtaining more sodium in geopolymer systems when Ca^{+2} balances the negative charge of $Al(OH)^{-}_4$, this means that presence of Ca could enhance mechanical strength (Rashidian and Rangaraju 2017).

Therefore, the effect of TIPA was significant in the highest compressive strength achieved, as 0.05% TIPA was used in 5% SW samples to achieve such strength. The effect of TIPA was also noticed in the highest flexural strength which was attained using 0.1% TIPA in 0% SW samples. Going foward, the study concentrates on the characterization of 5%SW samples due to its high mechanical properties.

4.3 Isothermal calorimetry

Exothermic peaks were observed during the reaction of the mixes observed through calorimetry results shown in Fig. 21, these periods include the initial reaction, slow reaction, period of acceleration, and finally, period of deceleration. The increase from the initial reaction showed the emergence of the earliest exothermic peak from the heat evolved when the precursors were wetted and dissolved with water. This correlates to the absorption of the alkali activating solution on the top of the particles which corresponds to the initial dissolution step (Buchwald et al. 2009). Other slow period relates to the induction period, when the Al-O and Si-O bonds on the particles surface were attacked by OH- anions, causing them to split in the aqueous solution and then giving way for aluminosilicate units to form, and as well, enable complexation reaction with the alkaline ions (Yao et al. 2009, Ravikumar and Neithalath 2012). The acceleration period correlates to the phase of continued dissolution where breakdown of Si-O-Al-O species occurred (Vassalo et al. 2014) leading to the phase of reaction-precipitation where the formation of aluminosilicates hydrate gel (C-S-H) results in the high exothermic peak (Duxson, Fernández-Jiménez, et al. 2007). The uniform drop in the peak can be linked with the release of water (Hamzaoui et al. 2015) at the time of polymerization.

The largest exothermic peak was measured at 23.9 mW/g, followed by 19.9 mW/g, 19.8 mW/g, and 18.5 mW/g for 5%SW, 5%SWa, 5%SWb, and 5%SWc respectively. The heat released curve of the four samples evolved similarly which is connected to the high alkalinity of the activating element in the activator powder which at the early activation stage, promoted the dissolution of alumino-silicate in the precursors, giving rise to nucleation, growth and finally the precipitation of the reaction product seen in the peak. The effect of TIPA was not significant in the heat evolution of the samples as the sample without TIPA recorded the highest peak, while a decreasing trend in peak was observed with subsequent addition of TIPA.

The cumulative heat flow of the pastes was similar at 90 hours. There seems to be no significant effect of TIPA addition on the heat released as 5% SW had higher heat released during the time frame studied. This may be due to the chelating effect of TIPA at the early stages of reaction. Meanwhile, sample with highest amount of TIPA (5% SWc) recorded the lowest cumulative heat flow at 124 J/g.

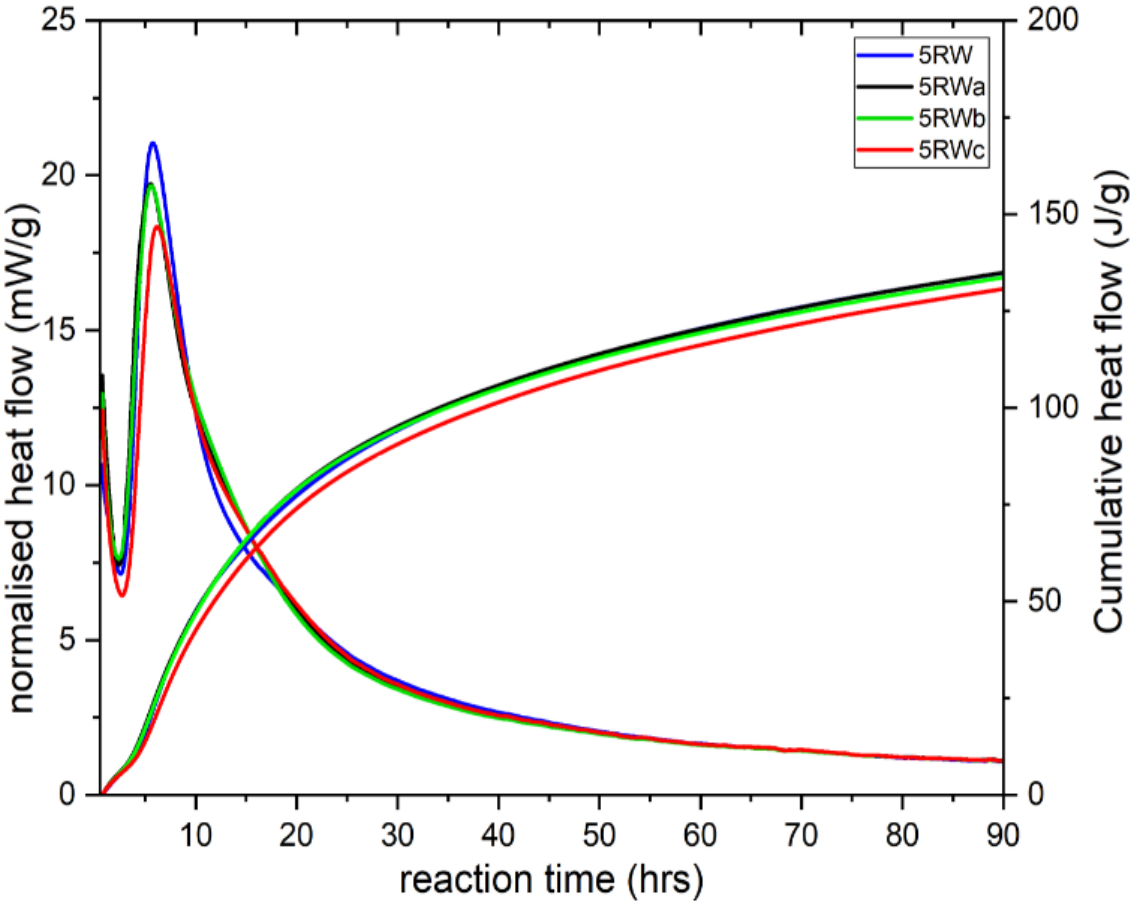

Figure 21. Iso-thermal calorimetry of 5% SW samples.

4.4 **Dissolution of BFS, SW and De-dust in NaOH**

Elemental compositions of raw materials involved in the chemical reactions that results in geopolymerization, originate from the amorphous silico-aluminate source, this reaction begins with the dissolution of aluminum and silicon in alkaline solution. Their degree of dissolution is therefore important for the subsequent polycondensation, and can highly aid in the mechanical and physical features of the final product (Liguori et al. 2017). Fig. 22 below shows the percentage rate of the dissolution of silicon (Si), aluminium (Al),

calcium (Ca) and iron (Fe) in all 5% SW samples. Silicon had the highest degree of dissolution at 52.4%, followed by aluminum at 34.7%, while the dissolution of calcium and iron was significantly low at 0.1%.

The dissolution rate of aluminosilicates was higher in all samples because of the concentration of NaOH solution. A higher concentration (3-7 M) has been found to accelerate the dissolution of aluminosilicates species as reported by (Liguori et al. 2017). The high alkaline medium in this test which ranged between 12.1 to 12.3 aided in the dissolution of these elements, this correlates with the report by Kinnunen et al 2017 on the high solubility of SW at pH 11.6. The very low dissolution rate of Ca and Fe could be linked to the formation of oxides of calcium which mainly dissolve in acid medium (Zieglar et al. 2016), and as well, the formation of iron hydroxide ($(Fe(OH)_2$ and/or $Fe(OH)_3$) in the test condition, resulting to their precipitation from the sample during the alkali dissolution, hence yielding only insignificant amounts in the solution (Sreenivasan et al. 2017, Adesanya et al. 2020).

The reduced dissolution of Si and Al after addition of TIPA could be attributed to the expected enhanced dissolution of Fe which stoichiometrically was not included in the filtrate due to formation of iron precipitates with the residual solute. The effect of TIPA on Fe dissolution in the binder phase have been previously reported (Zuo et al. 2018). However, in 5%SWc, the degree of dissolution of aluminum rose significantly, attributed to the increased amount of TIPA on aluminum dissolution.

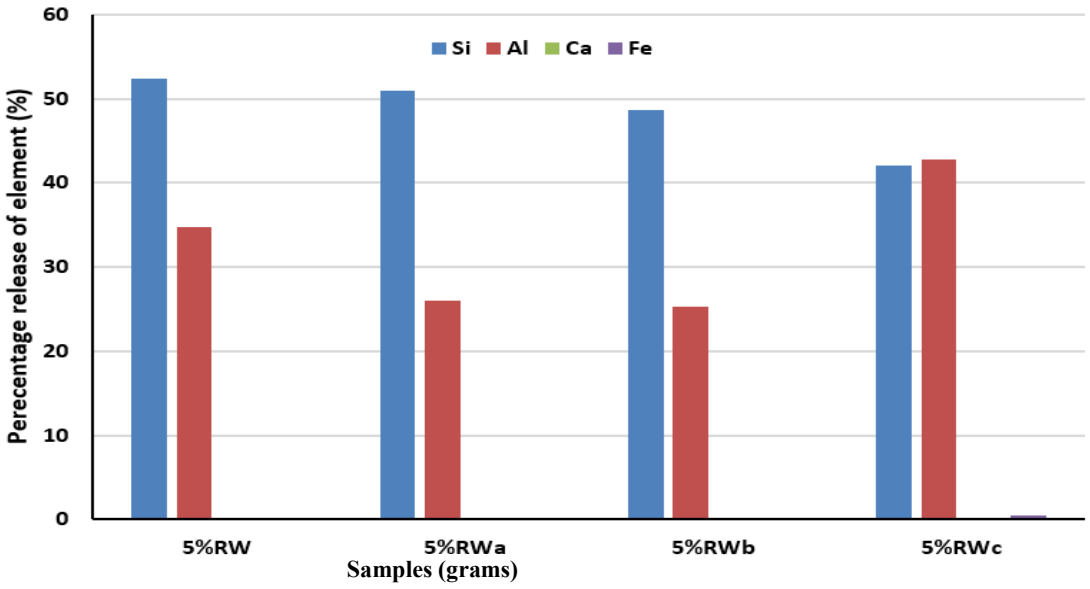

Figure 22. Dissolution rate of Si, Al, Ca, and Fe.

4.5 Quantitative x-ray diffraction (QXRD) of precursors

X-ray diffraction analysis was performed to identify the phase composition of the reaction products. As seen in Fig. 23a to 23d, different amounts of wollastontie-2M (W), hydrotalcite (HT) , clinotobermorite (C-S-H), Rutile (R) and calcite (C) were reflecetd in the peak characteristics. Rutile peaks are as a result of the internal standard added. The XRD patterns of days 7 and 28 samples showed no significant difference, which implied that the hydration reaction of the samples were almost concluded in the first 7 days and after that they reacted slowly. The analysis was prepared to quantify the reaction products as a function of curing time, however the quantification of C-S-H was not possible due to lack of coordination number. C-S-H is semi-crystalline. Hence, the observed mineralogy were not quantified. The main reaction product of the synthesis was C-S-H as seen in the Fig. 22. Similar observations have been reported with BFS alkali activation (Xing et al. 2019, Abdel Rahman et al. 2016).

Hydrotalcite phase was also observed as a reaction product, this is due to higher amount of MgO contained in the precursors precisely BFS and SW. Yliniemi et al. (2016) reported a hydrotalcite-type magnesium phase indicating the reaction of magnesium content from SW with CO_2, thereby standing in as a sorbent for CO_2 during the binders formation (Yliniemi et al. 2016). Bernal et al. (2013) reported similar phase in alkali activation of BFS (Bernal, San Nicolas, et al. 2014). Hydrotalcite is also present in AAS binder as a hydrous alkali earth aluminate phase which can be carbonated under all exposure conditions (Bernal et al. 2013).

Traces of calcium carbonate (Calcite) were detected as well, and could be as a result of the CO_2 absorbed from air during sample analysis (Mobasher et al. 2016). The X-ray diffractogram also detected crystalline phase of a natural ore and a rare reactive silicate; Wallastonite-2M, which is also a dehydration product of C-S-H gel it can be carbonated to calcium carbonate, its conversion rate however depends on temperature (Svensson et al. 2018).

(a) **5% SW**

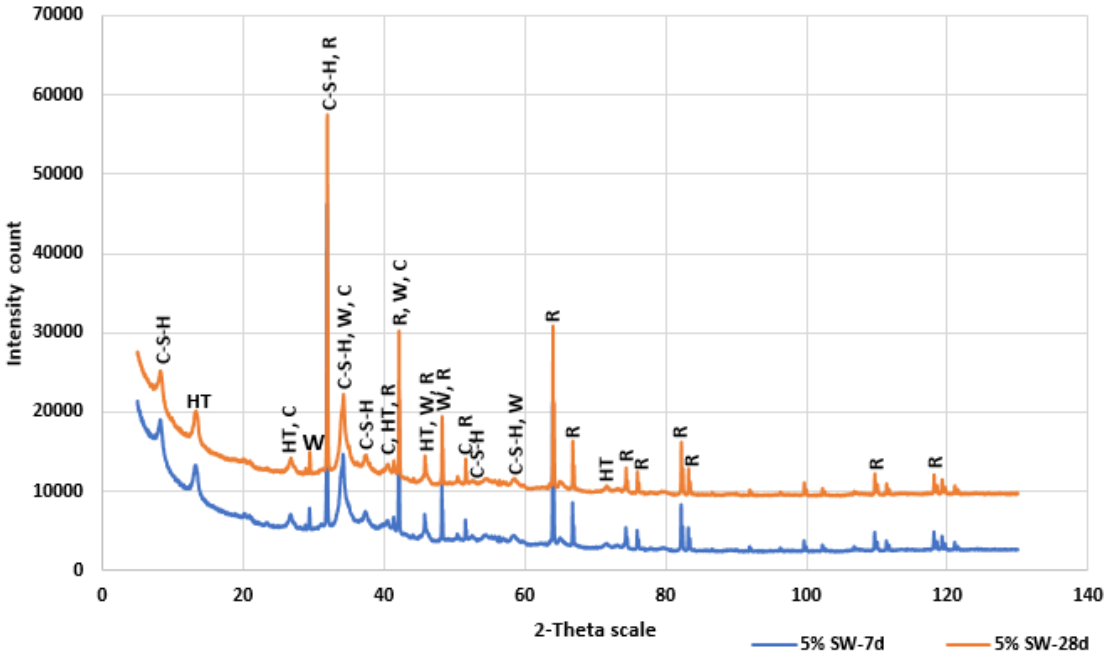
Intensity count
2-Theta scale
5% SW-7d
5% SW-28d
C-S-H
HT
HT, C
W
C-S-H, R
C-S-H, W, C
C-S-H
C, HT, R
R, W, C
HT, W, R
W, R
C, R
C-S-H
C-S-H, W
R
HT
R
R
R
R
R

(b) **5% SWa**

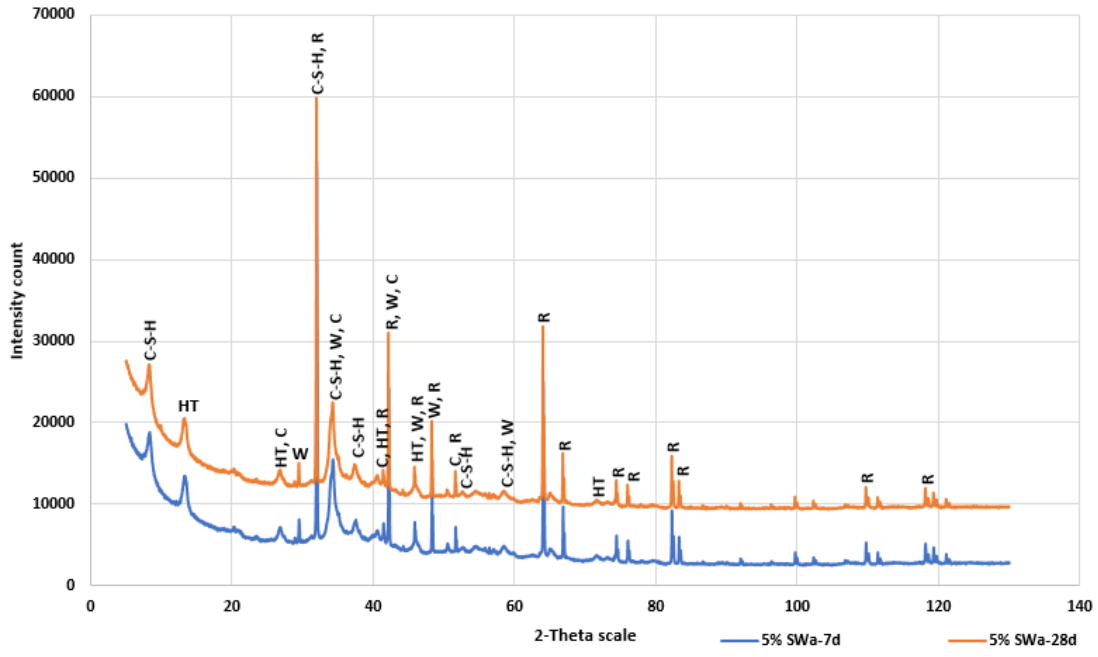
Intensity count
2-Theta scale
5% SWa-7d
5% SWa-28d
C-S-H
HT
HT, C
W
C-S-H, R
C-S-H, W, C
C-S-H
C, HT, R
R, W, C
HT, W, R
W, R
C, R
C-S-H
C-S-H, W
R
HT
R
R
R
R
R

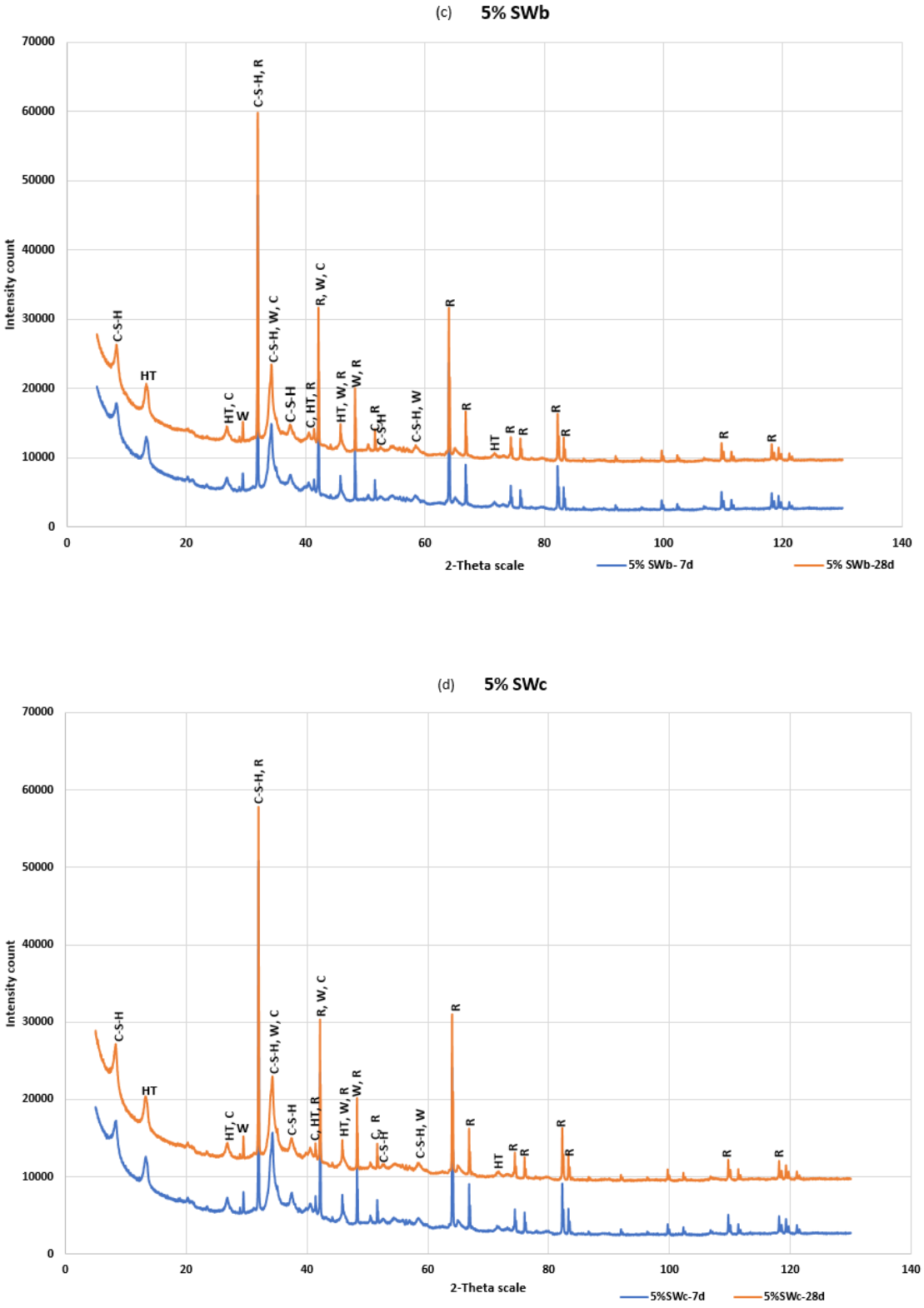

Figure 23. X-ray Diffraction of alkali activated binders at 7 and 28 days for (a) 5% SW (b) 5% SWa (c) 5% SWb (d) 5% SWd. Where R= rutile, W= wollastontie-2M, HT= hydrotalcite, (C-S-H)= clinotobermorite and C= calcite.

4.6 Thermogravimetry and differential analysis (TGA/DTG)

The TG and DTG curves of 5% SW samples were chosen to explain the thermogravimetric behaviour of the AAMs. The curves as seen in Fig. 24 displayed various trends in the weight loss of the precursors. All samples in the 5% SW category recorded major DTG peaks between 107 to 300ºC which constitutes decomposition of the main reaction products; calcium silicate hydrate (C-S-H)**.** This correlates to the literature findings in alkali activated BFS, reporting the dehydration of C-S-H type gel between 180 to 300ºC (Alarcon-Ruiz et al. 2005) and 150 to 300ºC (Gao et al. 2015) respectively. Additionally, the weight loss in AAMs is usually characterized by different changes in weight loss, where the first stage is mostly presented by loss of the interlayer water or the adsorbed water of C-S-H (Türker et al. 2016, Zhang et al. 2016), ettringite decomposition (Park et al. 2016), and the process of C-S-H and C-A-S-H gel phase dehydroxylation (Niklioć et al. 2016, Dludlu et al. 2017).

The weight loss detected at a minor peak between 300-400ºC could be ascribed to the dehydration of hydrotalcite, similar results was recorded by (Yahyaoui et al. 2018 and Xing et al. 2019), and the minor peak detected in the curve between 520-680ºC could be correlated to the decarbonation of calcite, similar result was reported by (Bernal et al. 2015).Also, samples with 0.1% TIPA (5% SWb) was found with the lowest peak, followed by samples with 0.15% TIPA (5% SWc), this may suggest increased formation of reaction products as a result of the increased amount of TIPA which may have facilitated increased dissolution of the precursors. This is consistent with the strength result achieved in Fig. 19 and 20.

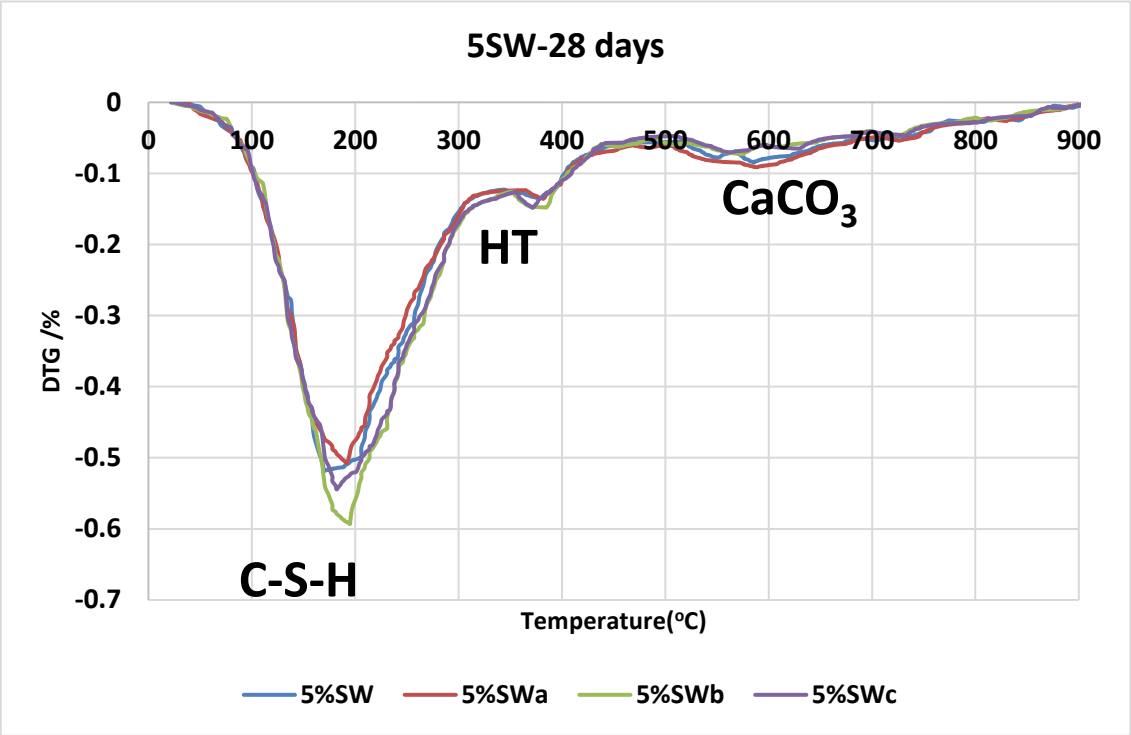

Figure 24. Thermogravimetry (TG) and Differential thermogravimetry (DTG) curves of 5% SW samples at 28 days of curing.

4.7 **Efflorescence of mortar**

Optical observation of the durability of the mortars was spotted after 48 hours (2 days) of subjecting the mortars to efflorescence test. Efflorescence was discovered in all the 16 samples which were categorised based on the percentage of SW (0% SW, 5% SW, 10% SW, and 15% SW). Appearance of efflorescence on all the SW range of samples which surfaced after 48 hours (day 2) was uniform and consistent. The reason for the uniformity in the appearance of efflorescence in all the samples could be as a result of the equal amount of high wt (g) of sodium in the De-dust. The samples in Fig. 25 were randomly chosen to show the level of efflorescence observed. There was no specification as regards %SW range because all samples exhibited similar trend in efflorescence.

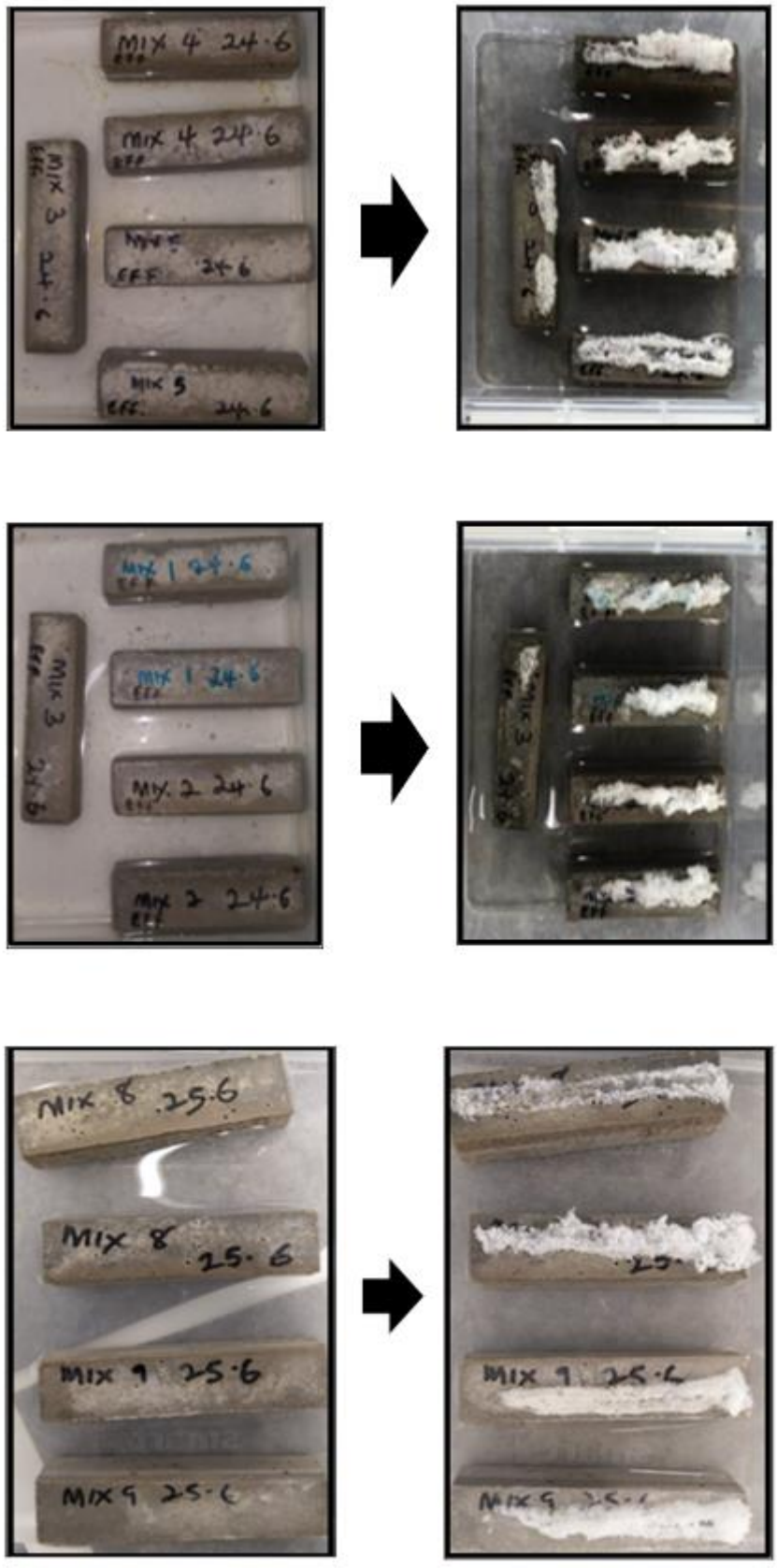

Figure 25. Efflorescent samples

5 Summary and conclusion

This experimental research aimed at establishing the possibility of using an industrial by-product known as desulphurization dust as an alternative alkali activator for the production of alkali activated binders, using blast furnace slag and stone wool as the main precursors. An efficient method known as "One-Part mix pathway" was employed in achieving this aim. Prerequisite preparations involved; size reduction of stone wool and determination of particle size distribution of all materials.

Determining the effectiveness of the alternative activating material was mostly achieved by keeping the mass ratio constant in all the experimental mixtures. Water to binder (w/b) ratio was also kept constant, while SiO_2/CaO, Na_2O/Al_2O_3, and $SiO2/Al_2O_3$ ratios were varied. Also, TIPA was incorporated to aid in the reactions. Product of these reactions were analyzed after 7 and 28 days.

Based on the experimental results, the following conclusion can be made:

- Desulphurization dust provided adequate activating properties required for alkali activation of the precursors, as its constant ratio in all mixtures provided ease of dissolution of minerals, resulting to moderate workability, increased strength, and high setting time.
- Stone wool is an appropriate co-binder to blast furnace slag as its solubility properties helped in the improvement of workability and strength of the mortars.
- Addition of 5% stone wool is considered the optimal amount for producing desired geopolymer mortars. This amount yielded the following; highest dissolution rates of Si and Al, highest workability, highest compressive strength and highest flexural strength.
- Addition of higher amount of stone wool reduced the strength, as lowest compressive strength was recorded in 10% stone wool samples.
- Also, higher amount of stone wool increased setting time, this was evident in samples with 10% and 15 % stone wool

Addition of TIPA presented significant effect in the following areas:

- In the workability of the pastes, samples with 0.1% TIPA recorded the highest flow percent.
- Regarding setting time of the geopolymer pastes, higher amount of TIPA (0.15%) did not have an effect at high stone wool content (10% and 15 %),
- The effectiveness of TIPA was also significantly observed in the compressive and flexural strength. The highest compressive strength was recorded from samples with 0.05% TIPA with 5% stone wool, while highest flexural strength was observed from samples with 0.1 % TIPA without stone wool.

Generally, the alkali content of the De-dust produced a consistent degree of efflorescence on the mortars.

5.1 Recommendations

Although the aims and objectives of this study was accomplished, however, further examination of other available materials is important in order to maximize the use of industrial by-product or wastes as an alternative alkali activator and precursors. It is also necessary to further this research using ambient temperature curing method, which is more energy efficient.

The availability and abundance of these industrial wastes or by-products is another important factor to consider ensuring its sustainable use for construction purposes.

6 References

Abdalqader, A. F., Jin, F., and Al-Tabbaa, A., 2016. Development of greener alkali-activated cement: utilisation of sodium carbonate for activating slag and fly ash mixtures. *Journal of Cleaner Production* , 113, 66–75. Available from:

Abdel-Gawwad, H. A. and Abo-El-Enein, S. A., 2016. A novel method to produce dry geopolymer cement powder. *HBRC Journal*, 12 (1), 13–24.

Abdel Rahman, A., Abo-El-Enein, S.A., Aboul-Fetouh, A., Shehata, Kh., 2016. Characteristics of Portland blast-furnace slag cement containing cement kiln dust and active silica. *Arabian Journal of Chemistry*, 9, S138–S143

Adesanya, E., 2015. Fibre-reinforced mineral wool geopolymer composites. *University of Oulu, Faculty of Technology, Environmental Engineering, master's thesis.* Available from: http://urn.fi/URN:NBN:fi:oulu-201506271885. [Accessed 15 Aug 2019]

Adesanya, E., Ohenoja, K., Luukkonen, T., Kinnunen, P., Illikainen, M., 2018. One-part geopolymer cement from slag and pretreated paper sludge. Journal of Cleaner Produc-tion, 185, 168-175Alarcon-Ruiz, L., Platret, G., Massieu, E., and Ehrlacher, A., 2005. The use of thermal analysis in assessing the effect of temperature on a cement paste. *Cement and Concrete Research*, 35 (3), 609–613.

Adesanya, E., Ohenoja, K., Yliniemi, J., Illikainen, M., 2020. Mechanical transformationof phyllite mineralogy toward its use as alkali activated binder precursor. Minerals Engineering, 145, 106093

Aldred, J. and Day, J., 2012. Is Geopolymer Concrete a Suitable Alternative To Traditional Concrete ? *37th Conference on Our World in Concrete & Structures*, (August), 1–14.

Ali, M. H., 1985. Fire resistant gypsum board containing mineral wool fibers and method. *United States Patent US4557973A* . Available from: https://patents.google.com/patent/US4557973. [Accessed 13 Jul 2019]

Allahverdi, A., Maleki, A., and Mahinroosta, M., 2018. Chemical activation of slag-blended Portland cement. *Journal of Building Engineering* , 18 , 76–83.

Alp, İ., Deveci, H., and Süngün, H., 2008. Utilization of flotation wastes of copper slag as raw material in cement production. *Journal of Hazardous Materials*, 159 (2–3), 390–395.

Alzaza, A., Mastali, M., Kinnune, P., Korat, L., Abdollahnejad, Z., Ducman, V., Illikainen, M., 2019. Production of lightweight alkali activated mortars using mineral wools. *Material, 12(10), 1695*

Antunes Boca Santa, R. A., Bernardin, A. M., Riella, H. G., and Kuhnen, N. C., 2013. Geopolymer synthetized from bottom coal ash and calcined paper sludge. *Journal of Cleaner Production*, 57, 302–307.

Arbi, K., Nedeljković, M., Zuo, Y., and Ye, G., 2016. A Review on the Durability of Alkali-Activated Fly Ash/Slag Systems: Advances, Issues, and Perspectives. *Industrial & Engineering Chemistry Research*, 55 (19), 5439–5453.

Assi, L. N., Eddie Deaver, E., and Ziehl, P., 2018. Effect of source and particle size distribution on the mechanical and microstructural properties of fly Ash-Based geopolymer concrete. *Construction and Building Materials*, 167, 372–380.

ASTM C1202-12, 2012. Standard Test Method for Electrical Indication of Concrete's Ability to Resist Chloride Ion Penetration, ASTM International, West Con-shohocken, PA, 7 pp.

ASTM C191-08, 2008, *Standard test methods for time of setting of hydraulic cement by Vicat needle*, American Society for Testing and Materials, Book of Standards Vol. 04.01,West Conshohocken, PA.

ASTM, C1437–15, Standard Test Method for Flow of Hydraulic Cement Mortar, ASTM International, West Conshohocken, PA, 2015.

Avirneni, D., Peddinti, P. R. T., and Saride, S., 2016. Durability and long term performance of geopolymer stabilized reclaimed asphalt pavement base courses. *Construction and Building Materials*, 121, 198–209.

Aydın, S. and Baradan, B., 2014. Effect of activator type and content on properties of alkali-activated slag mortars. *Composites Part B: Engineering*, 57, 166–172.

Barbosa, V. F. F. and MacKenzie, K. J. D., 2003. Synthesis and thermal behaviour of potassium sialate geopolymers. *Materials Letters*, 57 (9–10), 1477–1482.

Bernai, S. A., Gutierrez, R. M. De, and Rodríguez, E. D., 2013. Alkali-activated materials: cementing a sustainable future, 223 (2), 211–223.

Bernal, S. A., 2016. Advances in near-neutral salts activation of blast furnace slags. *RILEM Technical Letters*, 1, 39.

Bernal, S. A., de Gutierrez, R. M., Provis, J. L., and Rose, V., 2010. Effect of silicate modulus and metakaolin incorporation on the carbonation of alkali silicate-activated slags. *Cement and Concrete Research*, 40 (6), 898–907.

Bernal, S. A., Nicolas, R. S., Van Deventer, J. S. J., and Provis, J. L., 2016. Alkali-activated slag cements produced with a blended sodium carbonate/sodium silicate activator. *Advances in Cement Research*, 28 (4), 262–273.

Bernal, S. A., Provis, J. L., Fernández-Jiménez, A., Krivenko, P. V., Kavalerova, E., Palacios, M., and Shi, C., 2014. Binder Chemistry – High-Calcium Alkali-Activated Materials. In Alkali Activated Materials—State-of-the Art Report; Springer: Rotterdam, Netherlands, 59–91. Available from: http://link.springer.com/10.1007/978-94-007-7672-2_3 [Accessed 30 Jul 2019].

Bernal, S. A., Provis, J. L., Rose, V., and Mejía de Gutierrez, R., 2011. Evolution of binder structure in sodium silicate-activated slag-metakaolin blends. *Cement and Concrete Composites*, 33 (1), 46–54.

Bernal, S. A., Provis, J. L., Walkley, B., San Nicolas, R., Gehman, J. D., Brice, D. G., Kilcullen, A. R., Duxson, P., and van Deventer, J. S. J., 2013. Gel nanostructure in alkali-activated binders based on slag and fly ash, and effects of accelerated carbonation. *Cement and Concrete Research*, 53, 127–144.

Bernal, S. A., Rodríguez, E. D., Kirchheim, A. P., and Provis, J. L., 2016. Management and valorisation of wastes through use in producing alkali-activated cement materials. *Journal of Chemical Technology & Biotechnology*, 91 (9), 2365–2388.

Bernal, S. A., Rodríguez, E. D., Mejía de Gutiérrez, R., Gordillo, M., and Provis, J. L., 2011. Mechanical and thermal characterisation of geopolymers based on silicate-activated metakaolin/slag blends. *Journal of Materials Science*, 46 (16), 5477–5486.

Bernal, S. A., Rodríguez, E. D., Mejía de Gutiérrez, R., and Provis, J. L., 2015. Performaance at high temperature of alkali-activated slag pastes produced with silica fume and rice husk based activators. *Materiales De Construccion*, 65 (318), e049.

Bernal, S. A., Rodríguez, E. D., Mejia de Gutiérrez, R., Provis, J. L., and Delvasto, S., 2012. Activation of Metakaolin/Slag Blends Using Alkaline Solutions Based on Chemically Modified Silica Fume and Rice Husk Ash. *Waste and Biomass Valorization*, 3 (1), 99–108.

Bernal, S. A., San Nicolas, R., Myers, R. J., Mejía de Gutiérrez, R., Puertas, F., van Deventer, J. S. J., and Provis, J. L., 2014. MgO content of slag controls phase evolution and structural changes induced by accelerated carbonation in alkali-activated binders. *Cement and Concrete Research*, 57, 33–43.

Bernard de Quervain, 2011. *Resource Efficiency in Cement Production*. Smart Energy Strategies Conference 2011, Zurich, Switzerland, 22 September. Available from:

https://video.ethz.ch/conferences/2011/ses/2011-09-22/29b1ce23-fdd6-4b71-9a75-785bf6898b7f.html [Accessed 13 Aug 2019].

Bourguiba, A., Ghorbel, E., Cristofol, L., and Dhaoui, W., 2017. Effects of recycled sand on the properties and durability of polymer and cement based mortars. *Construction and Building Materials*, 153, 44–54.

Bouzón, N., Payá, J., Borrachero, M. V., Soriano, L., Tashima, M. M., and Monzó, J., 2014. Refluxed rice husk ash/NaOH suspension for preparing alkali activated binders. *Materials Letters*, 115, 72–74.

Brough, A. . and Atkinson, A., 2002. Sodium silicate-based, alkali-activated slag mortars: Part I. Strength, hydration and microstructure. *Cement and Concrete Research*, 32 (6), 865–879.

Buchwald, A., Tatarin, R., and Stephan, D., 2009. Reaction progress of alkaline-activated metakaolin-ground granulated blast furnace slag blends. *Journal of Materials Science*, 44 (20), 5609–5617.

Cadotte, J. E., 1970. Production of water-laid felted mineral fiber panels including use of flocculating agent. *United States Patent US3510394A*. Available from: https://patents.google.com/patent/US3510394.

Carrasco, T. M. and Puertas, F., 2017. Alkaline activation of different aluminosilicates as an alternative to Portland cement: Alkali activated cements or geopolymers. *Revista Ingenieria de Construccion*, 32 (2), 5–12.

Cheng, A., Lin, W. T., and Huang, R., 2011. Application of rock wool waste in cement-based composites. *Materials and Design* , 32 (2), 636–642.

Cheng, T. W., Lee, M. L., Ko, M. S., Ueng, T. H., and Yang, S. F., 2012. The heavy metal adsorption characteristics on metakaolin-based geopolymer. *Applied Clay Science*, 56, 90–96.

Chi, M., 2016. Mechnical strength and durability of alkali-activated fly ash/slag concrete. *Journal of Marine Science and Technology (Taiwan)*, 23 (5), 958–967.

Collins, F. and Sanjayan, J., 2000. Effect of pore size distribution on drying shrinking of alkali-activated slag concrete. *Cement and Concrete Research*, 30 (9), 1401–1406.

Criado, M., Walkley, B., Ke, X., Provis, J., Bernal, S., Criado, M., Walkley, B., Ke, X., Provis, J. L., and Bernal, S. A., 2018. Slag and Activator Chemistry Control the Reaction Kinetics of Sodium Metasilicate-Activated Slag Cements. *Sustainability*, 10 (12), 4709.

Cristelo, N., Miranda, T., Oliveira, D. V., Rosa, I., Soares, E., Coelho, P., and Fernandes,

L., 2015. Assessing the production of jet mix columns using alkali activated waste based on mechanical and financial performance and CO2 (eq) emissions. *Journal of Cleaner Production*, 102, 447–460.

Crossin, E., 2015. The greenhouse gas implications of using ground granulated blast furnace slag as a cement substitute. *Journal of Cleaner Production*, 95, 101–108.

Davidovits, J., 2008. *Geopolymer chemistry and applications*. Geopolymer Institute, 2008. Available from: https://books.google.com/books?hl=en&lr=&id=dliw_KTYq4oC&oi=fnd&pg=PA1&ots=GSk1oHqvn1&sig=7RTp7zfggkbltPogZ8xBQqEPOw0 [Accessed 21 Aug 2019].

Davidovits, J., 2015. Geopolymer Chemistry & Applications, 4th ed., Institut Geopolymere, Saint-Quentin, 558–568.

Deschner, F., Winnefeld, F., Lothenbach, B., Seufert, S., Schwesig, P., Dittrich, S., Goetz-Neunhoeffer, F., and Neubauer, J., 2012. Hydration of Portland cement with high replacement by siliceous fly ash. *Cement and Concrete Research*, 42 (10), 1389–1400.

Dimas, D., Giannopoulou, I., and Panias, D., 2009. Polymerization in sodium silicate solutions: A fundamental process in geopolymerization technology. *Journal of Materials Science*, 44 (14), 3719–3730.

Dludlu, M. K., Oboirien, B., and Sadiku, R., 2017. Micostructural and Mechanical Properties of Geopolymers Synthesized from Three Coal Fly Ashes from South Africa. *Energy & Fuels*, 31 (2), 1712–1722.

Dunster, A. M., 2007. Characterisation of mineral wastes, resources and processing technologies—Integrated waste management for production of construction material. Case Study: waste mineral fiber in ceiling tile manufacture, 1–7. Available from:http://www.smartwaste.co.uk/%0Afilelibrary/Ceiling_tiles_waste_mineral_wool.pdf.

Duxson, P., Fernández-Jiménez, A., Provis, J. L., Lukey, G. C., Palomo, A., and van Deventer, J. S. J., 2007a. Geopolymer technology: the current state of the art. *Journal of Materials Science*, 42 (9), 2917–2933.

Duxson, P. and Provis, J. L., 2008. Designing Precursors for Geopolymer Cements. *Journal of the American Ceramic Society*, 91 (12), 3864–3869.

Duxson, P., Provis, J. L., Lukey, G. C., and van Deventer, J. S. J., 2007. The role of

inorganic polymer technology in the development of ‘green concrete’. *Cement and Concrete Research*, 37 (12), 1590–1597.

Escalante-Garcia, J. I., Espinoza-Perez, L. J., Gorokhovsky, A., and Gomez-Zamorano, L. Y., 2009. Coarse blast furnace slag as a cementitious material, comparative study as a partial replacement of Portland cement and as an alkali activated cement. *Construction and Building Materials*, 23 (7), 2511–2517.

EN 197 1:2000, 2000. Cement. Part 1: Composition, Specifications and Conformity Criteria for Common Cements. European Committee for Standardization, Brussels, Belgium.

European Commision, 2015. Closing the loop - An EU action plan for the Circular Economy. *EU publications*, COM(2015). Available from: https://eur-lex.europa.eu/legal-content/EN/TXT/?uri=CELEX%3A52015DC0614#document2. [Accessed 17 August 2019].

European Commission, 2012. Europe 2020: Europe’s growth strategy. *EU publications*, NA-70-12-0. Available from: https://publications.europa.eu/en/publication-detail/-/publication/88ebf403-b2b1-40ab-adbb-c95b0c26ecee/language-es. [Accessed 21 Jul 2019].

European Commission, 2007.Integrated Pollution Prevention and Control. *In*: *Reference Document on Best Available Techniques for the Manufacture of Large Volume Inorganic Chemicals - Solids and Others industry*. Available from: https://eippcb.jrc.ec.europa.eu/reference/BREF/lvic-s_bref_0907.pdf [Accessed 21 Sep 2019].

Felaji, J. J. and Kehrer, K. P., 1990. Composite fiberboard and process of manufacture. *United States patent US4963603A* [online]. Available from: https://patents.google.com/patent/US4963603. [Accessed 15 Aug 2019].

Feng, D., Provis, J. L., and Deventer, J. S. J., 2012. Thermal Activation of Albite for the Synthesis of One-Part Mix Geopolymers. *Journal of the American Ceramic Society*, 95 (2), 565–572.

Fernández-Jiménez, A., Cristelo, N., Miranda, T., and Palomo, Á., 2017. Sustainable alkali activated materials: Precursor and activator derived from industrial wastes. *Journal of Cleaner Production*, 162, 1200–1209.

Fernández-Jiménez, A., Palomo, J. G., and Puertas, F., 1999. Alkali-activated slag mortars: Mechanical strength behaviour. *Cement and Concrete Research*, 29 (8),

1313–1321.

Fernández-Jiménez, A., Puertas, F., Sobrados, I., and Sanz, J., 2003. Structure of Calcium Silicate Hydrates Formed in Alkaline-Activated Slag: Influence of the Type of Alkaline Activator. *Journal of the American Ceramic Society*, 86 (8), 1389–1394.

Fernández Carrasco, L., Fernández-Giménez, A., and Palomo, A., 2007. Alkali activation of "Pozzolan-calcium aluminate cement" mixtures. *12th International Congress on the Chemistry of Cements* [online]. Available from: https://upcommons.upc.edu/handle/2117/22955 [Accessed 8 Oct 2019].

Fernández Jiménez, A., Flores, E., Maltseva, O., García-lodeiro, I., and Palomo, Á., 2013. Hybrid alkaline cements. Part III. Durability and industrial application. *Romanian Journal of Materials*, 43 (2), 195–200.

Fu, X., Hou, W., Yang, C., Li, D., and Wu, X., 2000. Studies on Portland cement with large amount of slag. *Cement and Concrete Research*, 30 (4), 645–649.

Gao, X., Yu, Q. L., and Brouwers, H. J. H., 2015. Reaction kinetics, gel character and strength of ambient temperature cured alkali activated slag–fly ash blends. *Construction and Building Materials*, 80, 105–115.

Gao, X., Yu, Q. L., Lazaro, A., and Brouwers, H. J. H., 2017. Investigation on a green olivine nano-silica source based activator in alkali activated slag-fly ash blends: Reaction kinetics, gel structure and carbon footprint. *Cement and Concrete Research*, 100, 129–139.

Garcia-Lodeiro, I., Palomo, A., and Fernández-Jiménez, A., 2014. *Crucial insights on the mix design of alkali-activated cement-based binders*. Handbook of Alkali-Activated Cements, Mortars and Concretes. Woodhead Publishing Limited. Available from: http://dx.doi.org/10.1533/9781782422884.1.49. [Accessed 22 June 2019].

Gartner, E. and Myers, D., 1993. Influence of Tertiary Alkanolamines on Portland Cement Hydration. *Journal of the American Ceramic Society*, 76 (6), 1521–1530.

Ghosh, K. and Ghosh, P., 2012. Effect Of Na2o/Al2o3, Sio2/Al2o3 And W/B Ratio On Setting Time And Workability Of Flyash Based Geopolymer. *International Journal of Engineering Research and Applications (IJERA) ISSN: 2248-9622*, 2, 2142–2147.

Gluth, G. J. G., Lehmann, C., Rübner, K., and Kühne, H.-C., 2013. Geopolymerization of a silica residue from waste treatment of chlorosilane production. *Materials and Structures*, 46 (8), 1291–1298.

Görhan, G. and Kürklü, G., 2014. The influence of the NaOH solution on the properties of the fly ash-based geopolymer mortar cured at different temperatures. *Composites*

Part B: Engineering, 58, 371–377.

Habert, G., D'Espinose De Lacaillerie, J. B., and Roussel, N., 2011. An environmental evaluation of geopolymer based concrete production: Reviewing current research trends. *Journal of Cleaner Production*, 19 (11), 1229–1238.

Habert, G. and Ouellet-Plamondon, C., 2016a. Recent update on the environmental impact of geopolymers. *RILEM Technical Letters*, 1, 17–23. Available from: http://letters.rilem.net/index.php/rilem/article/view/6 [Accessed 17 Aug 2019].

Hagerman, R. M., 1987. Mineral wool waste cement. *United States patent US4662941A*. Available from: https://patents.google.com/patent/US4662941. [Accessed 11 June 2019].

Haha, M. Ben, Lothenbach, B., Le Saout, G., and Winnefeld, F., 2011. Influence of slag chemistry on the hydration of alkali-activated blast-furnace slag — Part I: Effect of MgO. *Cement and Concrete Research*, 41 (9), 955–963.

Hajimohammadi, A., Ngo, T., Mendis, P., Kashani, A., and van Deventer, J. S. J., 2017. Alkali activated slag foams: The effect of the alkali reaction on foam characteristics. *Journal of Cleaner Production*, 147, 330–339.

Hajimohammadi, A., Provis, J. L., and van Deventer, J. S. J., 2010. Effect of Alumina Release Rate on the Mechanism of Geopolymer Gel Formation. *Chemistry of Materials*, 22 (18), 5199–5208.

Hajimohammadi, A., Provis, J. L., and van Deventer, J. S. J., 2011. The effect of silica availability on the mechanism of geopolymerisation. *Cement and Concrete Research*, 41 (3), 210–216.

Hamzaoui, R., Muslim, F., Guessasma, S., Bennabi, A., and Guillin, J., 2015. Structural and thermal behavior of proclay kaolinite using high energy ball milling process. *Powder Technology*, 271, 228–237.

Hardjito, D., Wallah, S. E., Sumajouw, D. M. J., and Rangan, B. V., 2004. On the Development of Fly Ash-Based Geopolymer Concrete. *ACI Materials Journal*, 101 (6), 467–472.

Heath, A., Paine, K., and McManus, M., 2014. Minimising the global warming potential of clay based geopolymers. *Journal of Cleaner Production*, 78, 75–83.

Heikal, M., Nassar, M. Y., El-Sayed, G., and Ibrahim, S. M., 2014. Physico-chemical, mechanical, microstructure and durability characteristics of alkali activated Egyptian slag. *Construction and Building Materials*, 69, 60–72.

Heinelt, W., 1996. Method and apparatus for treating mineral wool wastes. *European*

Patent EP0526697. B1. Available from: http://www.freepatentsonline.com/EP0526697.html [Accessed 10 Jul 2019].

Huang, H. and Shen, X., 2014. Interaction effect of triisopropanolamine and glucose on the hydration of Portland cement. *Construction and Building Materials*, 65, 360–366.

HUANG, H. and SHEN, X., 2011. Statistical study of cement additives with and without chloride on performance modification of Portland cement. *Progress in Natural Science: Materials International*, 21 (3), 246–253.

Hubler, M. H., Thomas, J. J., and Jennings, H. M., 2011. Influence of nucleation seeding on the hydration kinetics and compressive strength of alkali activated slag paste. *Cement and Concrete Research*, 41 (8), 842–846.

Humad, A. M., Provis, J. L., and Cwirzen, A., 2018. Alkali activation of a high MgO GGBS – fresh and hardened properties. *Magazine of Concrete Research.* 70, 1–24.

Jiřičková, M. and Černý, R., 2006. Effect of hydrophilic admixtures on moisture and heat transport and storage parameters of mineral wool. *Construction and Building Materials*, 20 (6), 425–434.

Kashani, A., Provis, J. L., Qiao, G. G., and van Deventer, J. S. J., 2014. The interrelationship between surface chemistry and rheology in alkali activated slag paste. *Construction and Building Materials*, 65, 583–591.

Kashani, A., Provis, J. L., Xu, J., Kilcullen, A. R., Qiao, G. G., and van Deventer, J. S. J., 2014. Effect of molecular architecture of polycarboxylate ethers on plasticizing performance in alkali-activated slag paste. *Journal of Materials Science*, 49 (7), 2761–2772.

Katsioti, M., Tsakiridis, P. E., Giannatos, P., Tsibouki, Z., and Marinos, J., 2009. Characterization of various cement grinding aids and their impact on grindability and cement performance. *Construction and Building Materials*, 23 (5), 1954–1959.

Ke, X., Bernal, S. A., Ye, N., Provis, J. L., and Yang, J., 2015. One-Part Geopolymers Based on Thermally Treated Red Mud/NaOH Blends. *Journal of the American Ceramic Society*, 98 (1), 5–11.

Kim, Y. J. and Choi, Y. W., 2012. Utilization of waste concrete powder as a substitution material for cement. *Construction and Building Materials*, 30, 500–504.

Kim, Y. Y., Lee, B.-J., Saraswathy, V., and Kwon, S.-J., 2014. Strength and durability

performance of alkali-activated rice husk ash geopolymer mortar. *The Scientific World Journal*, 2014, 209584. Available from: http://dx.doi.org/10.1155/2014/209584. [Accessed 21 Aug 2019].

Kinnunen, P., Yliniemi, J., Talling, B., and Illikainen, M., 2017a. Stonewool waste in fly ash geopolymer composites. *Journal of Material Cycles and Waste Management*, 19 (3), 1220–1227.

Kizinievič, O., Balkevičius, V., Pranckevičiene, J., and Kizinievič, V., 2014. Investigation of the usage of centrifuging waste of mineral wool melt (CMWW), contaminated with phenol and formaldehyde, in manufacturing of ceramic products. *Waste Management*, 34 (8), 1488–1494.

Kolani, B., Buffo-Lacarrière, L., Sellier, A., Escadeillas, G., Boutillon, L., and Linger, L., 2012. Hydration of slag-blended cements. *Cement and Concrete Composites*, 34 (9), 1009–1018.

Komnitsas, K. A., 2011. Potential of geopolymer technology towards green buildings and sustainable cities. *Procedia Engineering*, 21, 1023–1032.

Kovalchuk, G., Fernández-Jiménez, A., and Palomo, A., 2007. Alkali-activated fly ash: Effect of thermal curing conditions on mechanical and microstructural development – Part II. *Fuel*, 86 (3), 315–322.

Krivenko, P. V. and Kovalchuk, G. Y., 2007. Directed synthesis of alkaline aluminosilicate minerals in a geocement matrix. *Journal of Materials Science*, 42 (9), 2944–2952.

De la Paz, C., 2014. EU LIFE Programme: Contributing to waste management in Europe for over 20 years. *Waste Management*, 34 (3), 571–572.

Lazaro Garcia, A., 2014. Nano-silica production at low temperatures from the dissolution of olivine: synthesis, tailoring and modelling Eindhoven: Technische Universiteit Eindhoven. Available from: DOI: 10.6100/IR774494. [Accessed 23 Jun 2019]

Lee, C.-L., Huang, R., Lin, W.-T., and Weng, T.-L., 2012. Establishment of the durability indices for cement-based composite containing supplementary cementitious materials. *Materials & Design*, 37, 28–39.

Li, C., Sun, H. H., and Li, L. T., 2010a. Glass Phase Structure of Blast Furnace Slag. *Advanced Materials Research*, 168–170, 3–7.

Li, C., Sun, H., and Li, L., 2010b. A review: The comparison between alkali-activated slag (Si + Ca) and metakaolin (Si + Al) cements. *Cement and Concrete Research*, 40 (9), 1341–1349.

Li, Z., 2007. State of workability design technology for fresh concrete in Japan. *Cement and Concrete Research*, 37 (9), 1308–1320.

Liguori, B., Capasso, I., De Pertis, M., Ferone, C., and Cioffi, R., 2017. Geopolymerization ability of natural and secondary raw materials by solubility test in alkaline media. *Environments*, 4 (3), 56.

Lin, W.-T., Cheng, A., Huang, R., Chi, M.-C., and Hwang, H., 2011. Properties Evaluation of Cement-Based Composites Containing Steel Fiber and Silica Fume. *Advanced Science Letters*, 4 (3), 1155–1164.

Lin, W. T., Han, T. Y., Huang, C. C., Cheng, A., and Huang, R., 2012. Using rock wool wastes as partial replacement of cement in cement-based composites. *Advanced Science Letters*, 8, 489–494.

Liu, J., Yu, Q., Zuo, Z., Yang, F., Han, Z., and Qin, Q., 2019. Reactivity and performance of dry granulation blast furnace slag cement. *Cement and Concrete Composites*, 95, 19–24.

Lloyd, R. R., Provis, J. L., and van Deventer, J. S. J., 2012. Acid resistance of inorganic polymer binders. 1. Corrosion rate. *Materials and Structures*, 45 (1–2), 1–14.

Long, W. J., 1985. *Mineral fiber-containing paper for the production of gypsum wallboard product prepared therewith*. Canadian Patents Database. CA1192709A1. Available from: http://www.google.com/patents/CA1192709A1. [Accessed 10 Jul 2019].

Luukkonen, T., Abdollahnejad, Z., Yliniemi, J., Kinnunen, P., and Illikainen, M., 2018a. Comparison of alkali and silica sources in one-part alkali-activated blast furnace slag mortar. *Journal of Cleaner Production*, 187, 171–179.

Luukkonen, T., Abdollahnejad, Z., Yliniemi, J., Kinnunen, P., and Illikainen, M., 2018b. One-part alkali-activated materials: A review. *Cement and Concrete Research*, 103, 21–34.

Maghool, F., Arulrajah, A., Horpibulsuk, S., and Du, Y.-J., 2017. Laboratory Evaluation of Ladle Furnace Slag in Unbound Pavement-Base/Subbase Applications. *Journal of Materials in Civil Engineering*, 29 (2), 04016197.

Marchon, D., Sulser, U., Eberhardt, A., and Flatt, R. J., 2013. Molecular design of comb-shaped polycarboxylate dispersants for environmentally friendly concrete. *Soft Matter*, 9 (45), 10719-10728.

Martin, A., Pastor, J. Y., Palomo, A., and Fernández Jiménez, A., 2015. Mechanical behaviour at high temperature of alkali-activated aluminosilicates (geopolymers).

Construction and Building Materials, 93, 1188–1196.

Matalkah, F., Xu, L., Wu, W., and Soroushian, P., 2017. Mechanochemical synthesis of one-part alkali aluminosilicate hydraulic cement. *Materials and Structures*, 50 (1), 97.

McLellan, B. C., Williams, R. P., Lay, J., Van Riessen, A., and Corder, G. D., 2011. Costs and carbon emissions for geopolymer pastes in comparison to ordinary portland cement. *Journal of Cleaner Production*, 19 (9–10), 1080–1090.

Mejía, J. M., Mejía de Gutiérrez, R., and Puertas, F., 2013. Ceniza de cascarilla de arroz como fuente de sílice en sistemas cementicios de ceniza volante y escoria activados alcalinamente. *Materiales de Construcción*, 63 (311), 361–375.

Mellado, A., Catalán, C., Bouzón, N., Borrachero, M. V., Monzó, J. M., and Payá, J., 2014. Carbon footprint of geopolymeric mortar: study of the contribution of the alkaline activating solution and assessment of an alternative route. *RSC Adv.*, 4 (45), 23846–23852.

Memon, F.A., Nuruddin, M.F., Demie, S., and Shafiq, Nasir., 2011. Effect of curing conditions on strength of fly ash-based self-compacting geopolymer concrete. *International Journal of Civil and Environmental Engineering. 5, 8.*

Mobasher, N., Bernal, S. A., and Provis, J. L., 2016. Structural evolution of an alkali sulfate activated slag cement. *Journal of Nuclear Materials*, 468, 97–104.

Mohamed, O. A. and Najm, O. F., 2017. Compressive strength and stability of sustainable self-consolidating concrete containing fly ash, silica fume, and GGBS. *Frontiers of Structural and Civil Engineering*, 11 (4), 406–411.

Mohammed, B. S., Haruna, S., Wahab, M. M. A., Liew, M. S., and Haruna, A., 2019. Mechanical and microstructural properties of high calcium fly ash one-part geopolymer cement made with granular activator. *Heliyon*, 5 (9), e02255.

Moraes, J. C. B., Tashima, M. M., Akasaki, J. L., Melges, J. L. P., Monzó, J., Borrachero, M. V., Soriano, L., and Payá, J., 2016. Increasing the sustainability of alkali-activated binders: The use of sugar cane straw ash (SCSA). *Construction and Building Materials*, 124, 148–154.

Moseson, A. J., Moseson, D. E., and Barsoum, M. W., 2012. High volume limestone alkali-activated cement developed by design of experiment. *Cement and Concrete Composites*, 34 (3), 328–336.

Müller, A., Leydolph, B., and Stanelle, K., 2009. Recycling mineral wool waste—technologies for the conversion of the fiber structure part 1. *Interceram*, 378–381.

Nadoushan, M. J., Ramezanianpour, A. A., 2016. The effect of type and concentration of activators on flowability and compressive strength of natural pozzolan and slag-based geopolymers. *Construction and Building Materials,* 111, 337–347

Nath, P., and Sarker, P. K., 2014. Effect of BFS on setting, workability and early strength properties of fly ash geopolymer concrete cured in ambient condition. *Construction and Building Materials,* 66, 163–171

Nazari, A. and Sanjayan, J. G., 2016. *Handbook of low carbon concrete*. ButteSWorth-Heinemann. eBook ISBN: 9780128046404. Available at: https://www.elsevier.com/books/handbook-of-low-carbon-concrete/nazari/978-0-12-804524-4. [Accessed 7 Aug 2019].

Nematollahi, B., Sanjayan, J., and Shaikh, F. U. A., 2015. Synthesis of heat and ambient cured one-part geopolymer mixes with different grades of sodium silicate. *Ceramics International*, 41 (4), 5696–5704.

Niklioć, I., Marković, S., Janković – Častvan, I., Radmilović, V. V., Karanović, L., Babić, B., and Radmilović, V. R., 2016. Modification of mechanical and thermal properties of fly ash-based geopolymer by the incorporation of steel slag. *Materials Letters*, 176, 301–305.

Olivier, J. G. J., Janssens-Maenhout, G., and Peters, J. a H. W., 2012. *Trends in global CO2 emissions, PBL Netherlands Environmental Assessment Agency. 871.* Available from: http://dx.doi.org/10.2788/33777. [Accessed 23 Jun 2019].

Özbay, E., Erdemir, M., and Durmuş, H. I., 2016. Utilization and efficiency of ground granulated blast furnace slag on concrete properties - A review. *Construction and Building Materials*, 105, 423–434.

Pacheco-Torgal, F., Labrincha, J., Leonelli, C., Palomo, A., Chindaprasit, P., 2015. *Handbook of Alkali-Activated Cements, Mortars and Concretes*. Woodhead Publishing - Elsevier. Available from: https://linkinghub.elsevier.com/retrieve/pii/C20130165117 [Accessed 24 Jun 2019].

Pacheco-Torgal, F., Labrincha, J., Leonelli, C., and Palomo, A., 2015a. *Handbook of alkali-activated cements, mortars and concretes*. Woodhead Publishing Series in Civil Engineering and Construction. Available from: https://books.google.com/books?hl=en&lr=&id=KXQmBAAAQBAJ&oi=fnd&pg=PP1&ots=FHxv7i86T-&sig=G7BsxMolUZWP_zaC8RrmNc0Ylh4 [Accessed 31 Jul 2019].

Palomo, A., Krivenko, P., Garcia-Lodeiro, I., Kavalerova, E., Maltseva, O., Fernández-

Jiménez, A., and Fernández-Jiménez, A., 2014. A review on alkaline activation: new analytical perspectives. *Materiales de Construcción*, 64 (315), e022.

Papadopoulos, A. M., 2005. State of the art in thermal insulation materials and aims for future developments. *Energy and Buildings*, 37 (1), 77–86.

Papatzani, S. and Paine, K., 2015. 'Overview of construction and demolition waste legislation in EU and Greece & state of the art on recycling CDEW in concrete' Paper presented at Fifth International Conference on Environmental Management, Engineering, Planning and Economics (CEMEPE) and SECOTOX Conference, Myconos, Greece, 14/06/15 - 18/07/15. Available from: https://researchportal.bath.ac.uk/en/publications/overview-of-construction-and-demolition-waste-legislation-in-eu-a. [Accessed 13 Aug 2019]

Park, H., Jeong, Y., Jun, Y., Jeong, J.-H., and Oh, J. E., 2016. Strength enhancement and pore-size refinement in clinker-free CaO-activated BFS systems through substitution with gypsum. *Cement and Concrete Composites*, 68, 57–65.

Passuello, A., Rodríguez, E. D., Hirt, E., Longhi, M., Bernal, S. A., Provis, J. L., and Kirchheim, A. P., 2017. Evaluation of the potential improvement in the environmental footprint of geopolymers using waste-derived activators. *Journal of Cleaner Production*, 166, 680–689.

Peng, M. X., Wang, Z. H., Shen, S. H., and Xiao, Q. G., 2015. Synthesis, characterization and mechanisms of one-part geopolymeric cement by calcining low-quality kaolin with alkali. *Materials and Structures*, 48 (3), 699–708.

Peng, M. X., Wang, Z. H., Shen, S. H., Xiao, Q. G., Li, L. J., Tang, Y. C., and Hu, L. L., 2017. Alkali fusion of bentonite to synthesize one-part geopolymeric cements cured at elevated temperature by comparison with two-part ones. *Construction and Building Materials*, 130, 103–112.

Pranckevi, J., 2011. Impact of mineral wool production waste on properties of sintered ceramics. *Doctoral Dissertation. Vilnius Gediminas Technical University, Vilna, Lithuania*. Available from: https://leidykla.vgtu.lt/index.php?id_product=1318&id_product_attribute=0&rewrite=impact-of-mineral-wool-production-waste-on-properties-of-sintered-ceramics&controller=product&id_lang=1. [Accessed 21 Jul 2019].

Provis, J. L., 2014a. Geopolymers and other alkali activated materials: why, how, and what? *Materials and Structures*, 47 (1–2), 11–25.

Provis, J. L., 2014b. Green concrete or red herring? - Future of alkali-activated materials. *In*: *Advances in Applied Ceramics*. Maney Publishing, 472–477.

Provis, J. L., 2018. Alkali-activated materials. *Cement and Concrete Research* [online], 114, 40–48. Available from: https://doi.org/10.1016/j.cemconres.2017.02.009. [Accessed 25 Jul 2019]

Provis, J. L. and S. A. B., 2014c. *Binder chemistry – Blended systems and intermediate Ca content, in Alkali-Activated Materials: State-of-the-Art Report, RILEM TC 224-AAM*. Springer/RILEM: Dordrecht. Available from: https://www.rilem.net/global/gene/link.php?doc_id=3969&fg=1 [Accessed 24 Jul 2019].

Provis, J. L. and van Deventer, J. S. J., 2014. Alkali Activated Materials: State-of-the-Art Report, RILEM TC 224-AAM. [online], 13, 388. Available from: http://link.springer.com/10.1007/978-94-007-7672-2 [Accessed 31 Jul 2019].

Provis, J. L. and Van Deventer, J. S. J., 2009. *Geopolymers : structure, processing, properties and industrial applications*. Woodhead.

Provis, J. L. and Palomo, A., 2015. Advances in understanding alkali-activated materials. *Cement and Concrete Research*, 78, 110–125.

Pu, X., C. Yang, and C. G., 1992. Study on retardation of setting of alkali activated slag concrete. *Cement* , 10, 32–36.

Puertas, F., Martínez-Ramírez, S., Alonso, S., and Vázquez, T., 2000. Alkali-activated fly ash/slag cements: Strength behaviour and hydration products. *Cement and Concrete Research*, 30 (10), 1625–1632.

Puertas, F. and Torres-Carrasco, M., 2014a. Use of glass waste as an activator in the preparation of alkali-activated slag. Mechanical strength and paste characterisation. *Cement and Concrete Research*, 57, 95–104.

Rashad, A. M., 2013. A comprehensive overview about the influence of different additives on the properties of alkali-activated slag – A guide for Civil Engineer. *Construction and Building Materials*, 47, 29–55.

Rashad, A. M., Bai, Y., Basheer, P. A. M., Collier, N. C., and Milestone, N. B., 2012. Chemical and mechanical stability of sodium sulfate activated slag after exposure to elevated temperature. *Cement and Concrete Research*, 42 (2), 333–343.

Rashad, A. M. and Sadek, D. M., 2017. An investigation on Portland cement replaced by high-volume GGBS pastes modified with micro-sized metakaolin subjected to elevated temperatures. *International Journal of Sustainable Built Environment*, 6

(1), 91–101.

Rashidian-Dezfouli, H., Rangaraju, P.R., 2017. Comparison of strength and durability characteristics of a geopolymer produced from fly ash, ground glass fiber and glass powder. *Materiales de Construccion*. 67 (328), e136

Ravikumar, D. and Neithalath, N., 2012. Reaction kinetics in sodium silicate powder and liquid activated slag binders evaluated using isothermal calorimetry. *Thermochimica Acta*, 546, 32–43.

Reig, L., Tashima, M. M., Borrachero, M. V., Monzó, J., Cheeseman, C. R., and Payá, J., 2013. Properties and microstructure of alkali-activated red clay brick waste. *Construction and Building Materials*, 43, 98–106.

Rodríguez, E. D., Bernal, S. A., Provis, J. L., Paya, J., Monzo, J. M., and Borrachero, M. V., 2013. Effect of nanosilica-based activators on the performance of an alkali-activated fly ash binder. *Cement and Concrete Composites*, 35 (1), 1–11.

Roy, D. M., Jiang, W., and Silsbee, M. ., 2000. Chloride diffusion in ordinary, blended, and alkali-activated cement pastes and its relation to other properties. *Cement and Concrete Research*, 30 (12), 1879–1884.

Sadek, D. M., 2014. Effect of cooling technique of blast furnace slag on the thermal behavior of solid cement bricks. *Journal of Cleaner Production*, 79 (79), 134–141.

Sandberg, P. J. and Doncaster, F., 2004. On the mechanism of strength enhancement of cement paste and mortar with triisopropanolamine. *Cement and Concrete Research*, 34 (6), 973–976.

Shi, C., 2004. Effect of mixing proportions of concrete on its electrical conductivity and the rapid chloride permeability test (ASTM C1202 or ASSHTO T277) results. *Cement and Concrete Research*, 34 (3), 537–545.

Shi, C. and Day, R. L., 1995. A calorimetric study of early hydration of alkali-slag cements. *Cement and Concrete Research*, 25 (6), 1333–1346.

Shi, C., Krivenko, P. V., and Roy, D. M., 2006. *Alkali-activated cements and concretes* [online]. Taylor & Francis, Abingdon, The United Kingdom.

Shi, C. and Qian, J., 2000. High performance cementing materials from industrial slags — a review. *Resources, Conservation and Recycling*, 29 (3), 195–207.

Shi, C., Roy, D., and Krivenko, P., 2003. *Alkali-activated cements and concretes*. CRC Press: eBook ISBN9780429180712. Available from: https://doi.org/10.1201/9781482266900 [Accessed 26 Jul 2019].

Siddique, R. and Khan, M. I., 2011. *Supplementary Cementing Materials*. Berlin, Heidelberg: Springer Berlin Heidelberg. eBook ISBN 978-3-642-17866-5 Available from: http://link.springer.com/10.1007/978-3-642-17866-5 [Accessed 18 Jul 2019].

Singh, B., Ishwarya, G., Gupta, M., and Bhattacharyya, S. K., 2015. Geopolymer concrete: A review of some recent developments. *Construction and Building Materials*, 85, 78–90.

Somasundaran, P. and Shrotri, S., 1995. Grinding Aids: A Review of Their Use, Effect and Mechanisms. Selected Topics in Mineral Processing[M]. *London: Wiley Eastern Limited,* [online], 47–70. Available from: https://ci.nii.ac.jp/naid/10014704119/ [Accessed 3 Aug 2019].

Somna, K., Jaturapitakkul, C., Kajitvichyanukul, P., and Chindaprasirt, P., 2011. NaOH-activated ground fly ash geopolymer cured at ambient temperature. *Fuel*, 90 (6), 2118–2124.

Soutsos, M. N., Tang, K., and Millard, S. G., 2011. Use of recycled demolition aggregate in precast products, phase II: Concrete paving blocks. *Construction and Building Materials*, 25 (7), 3131–3143.

Sreenivasan, H., Kinnunen, P., Heikkinen, E., Illikainen, M., 2017. Thermally treated phlogopite as magnesium-rich precursor for alkali activation purpose. *Minerals Engineering*, 113, 47–54

Sturm, P., Gluth, G. J. G., Brouwers, H. J. H., and Kühne, H.-C., 2016. Synthesizing one-part geopolymers from rice husk ash. *Construction and Building Materials*, 124, 961–966.

Svensson, K., Neumann, A., Menezes, F. F., Lempp, C., and Pöllmann, H., 2018. The conversion of wollastonite to caco3 considering its use for ccs application as cementitious material. *Applied Science*, 8, 304.

Talling, B. and Sarudis, M., 1995. Raw material briquette for mineral wool production and process for its preparation and its use. *United States Patent US5472917A* [online]. Available from: http://www.google.com.ar/patents/US5472917. [Accessed 24 Jun 2019].

Tashima, M. M., Akasaki, J. L., Castaldelli, V. N., Soriano, L., Monzó, J., Payá, J., and Borrachero, M. V., 2012. New geopolymeric binder based on fluid catalytic cracking catalyst residue (FCC). *Materials Letters*, 80, 50–52.

Temuujin, J., Minjigmaa, A., Lee, M., Chen-Tan, N., and van Riessen, A., 2011. Characterisation of class F fly ash geopolymer pastes immersed in acid and alkaline solutions. *Cement and Concrete Composites*, 33 (10), 1086–1091.

Thomas, J. J., Allen, A. J., and Jennings, H. M., 2012. Density and water content of nanoscale solid C–S–H formed in alkali-activated slag (AAS) paste and implications for chemical shrinkage. *Cement and Concrete Research*, 42 (2), 377–383.

Tošić, N., Marinković, S., Pecić, N., Ignjatović, I., and Dragaš, J., 2018. Long-term behaviour of reinforced beams made with natural or recycled aggregate concrete and high-volume fly ash concrete. *Construction and Building Materials*, 176, 344–358.

Trabzuni, F. M.S., Dekki, H. M. El., and Gopalkrishnan, C. C., 2011. Process for hydrothermal production of sodium silicate solutions and precipitated silicas. United States Patent US20090022646A1. Available from: https://patents.google.com/patent/US20090022646A1/en [Accessed 9 Sep 2019].

Tsakiridis, P. E., Papadimitriou, G. D., Tsivilis, S., and Koroneos, C., 2008. Utilization of steel slag for Portland cement clinker production. *Journal of Hazardous Materials*, 152 (2), 805–811.

Türker, H. T., Balçikanli, M., Durmuş, İ. H., Özbay, E., and Erdemir, M., 2016. Microstructural alteration of alkali activated slag mortars depend on exposed high temperature level. *Construction and Building Materials*, 104, 169–180.

Turner, L. K. and Collins, F. G., 2013. Carbon dioxide equivalent (CO2-e) emissions: A comparison between geopolymer and OPC cement concrete. *Construction and Building Materials*, 43, 125–130.

Turu'allo, G., Kougioumtzoglou, I. A., and S.W. Jones, C., 2013. Early Age Strength Development of GGBS Concrete Cured under Different Temperatures. PhD thesis. Available from: https://livrepository.liverpool.ac.uk/12215/1/TurualloGid_Jun2013_12215.pdf. [Accessed 9 Jul 2019]

Väntsi, O. and Kärki, T., 2014. Mineral wool waste in Europe: a review of mineral wool waste quantity, quality, and current recycling methods. *Journal of Material Cycles and Waste Management*, 16 (1), 62–72.

Van Deventer, J. S. J., Provis, J. L., and Duxson, P., 2012. Technical and commercial progress in the adoption of geopolymer cement. *Minerals Engineering*, 29, 89–104.

Van Jaarsveld, J. G. S., Van Deventer, J. S. J., and Lorenzen, L., 1997. The potential use of geopolymeric materials to immobilise toxic metals: Part I. Theory and applications. *Minerals Engineering*, 10 (7), 659–669.

Vassalo, E. A. S., Gumieri, A. G., and Aguilar, M. T. P., 2014. Characterization of geopolymers obtained by alkaline activation of metakaolin with high iron content. *In*: Chantawarangul, K., Swanpaga, W., Yazdani, S., Vimonsatit, V. and, and Singh, A., eds. *Sustainable Solutions in Structural Engineering and Construction*. Thailand: ISEC Press, Volume 1 Issue 1. Available from: https://www.isec-society.org/ISEC_PRESS/ASEA-SEC_02/index.html [Accessed 9 Oct 2019].

Villoria Sáez, P., del Río Merino, M., and Porras-Amores, C., 2012. Estimation of construction and demolition waste volume generation in new residential buildings in Spain. *Waste Management & Research*, 30 (2), 137–146.

Vinai, R., Soutsos, M., 2019. Production of sodium silicate powder from waste glass cullet for alkali activation of alternative binders. *Cement and Concrete Research,* 116 45–56

Walling, S. A., Kinoshita, H., Bernal, S. A., Collier, N. C., and Provis, J. L., 2015. Structure and properties of binder gels formed in the system $Mg(OH)_2$–SiO_2–H_2O for immobilisation of Magnox sludge. *Dalton Transactions*, 44 (17), 8126–8137.

Wang, S.-D. and Scrivener, K. L., 1995. Hydration products of alkali activated slag cement. *Cement and Concrete Research*, 25 (3), 561–571.

Wang, S.-D., Scrivener, K. L., and Pratt, P. L., 1994. Factors affecting the strength of alkali-activated slag. *Cement and Concrete Research*, 24 (6), 1033–1043.

Weil, M., Dombrowski, K., Buchawald, A., 2009. *Life-cycle analysis of geopolymers*. Woodhead Publishing Limited Abington Hall, Cambridge.

Xing, J., Zhao, Y., Qiu, J., and Sun, X., 2019. Microstructural and mechanical properties of alkali activated materials from two types of blast furnace slags. *Materials*, 12 (13)2089.

Xu, H., 2002. Geopolymerisation of aluminosilicate minerals. PhD thesis, Department of Chemical Engineering, The University of Melbourne. Available from: http://hdl.handle.net/11343/38811. [Accessed 10 Aug 2019].

Xu, H. and Van Deventer, J. S. J., 2000a. The geopolymerisation of alumino-silicate minerals. *International Journal of Mineral Processing*, 59 (3), 247–266.

Xu, Z., Li, W., Sun, J., Hu, Y., Xu, K., Ma, S., and Shen, X., 2017. Research on cement hydration and hardening with different alkanolamines. *Construction and Building Materials*, 141, 296–306.

Yahyaoui, R., Jimenez, P.E.S., Maqueda, L.A.P., Nahdi, K., and Luque, J.M.C., 2018. Synthesis, characterization and combined kinetic analysis of thermal decomposition of hydrotalcite (Mg6Al2(OH)16CO3_4H2O). Thermochimica Acta, 667, 177–184

Yang, C. H., Wu, F., and Chen, K., 2011. Research on Set Retarder of High and Super High Strength Alkali -Activated Slag Cement and Concrete. *Key Engineering Materials*, 477, 164–169.

Yang, K.-H., Song, J.-K., and Song, K.-I., 2013. Assessment of CO_2 reduction of alkali-activated concrete. *Journal of Cleaner Production*, 39, 265–272.

Yao, X., Zhang, Z., Zhu, H., and Chen, Y., 2009. Geopolymerization process of alkali–metakaolinite characterized by isothermal calorimetry. *Thermochimica Acta*, 493 (1–2), 49–54.

Ye, H. and Radlińska, A., 2017. Effect of Alkalis on Cementitious Materials:Understanding the Relationship between Composition, Structure, and Volume Change Mechanism. *Journal of Advanced Concrete Technology*, 15 (4), 165–177.

Yliniemi, J., Kinnunen, P., Karinkanta, P., and Illikainen, M., 2016. Utilization of mineral wools as alkali-activated material precursor. *Materials*, 9 (5).

Zah, R. and Hischier, R., 2007. Life cycle inventories of detergents. *Final report ecoinvent data v2.0, No. 12. Swiss Centre for Life Cycle Inventories, Dübendorf, CH*. Available from: https://www.ecoinvent.org/database/older-versions/ecoinvent-version-2/reports-on-ecoinvent-2/reports-on-ecoinvent-2.html [Accessed 9 Sep 2019].

Zhang, H. Y., Kodur, V., Wu, B., Cao, L., and Wang, F., 2016. Thermal behavior and mechanical properties of geopolymer mortar after exposure to elevated temperatures. *Construction and Building Materials*, 109, 17–24.

Ziegler, D., Formia, A., Tulliani, J., and Palmero, P., 2016. Environmentally-friendly dense and porous geopolymers using fly ash and rice husk ash as raw materials. *Materials*. 9, 466

Zuo, F., Tan, H., He, X., Ma, B., Deng, X., Zhang, T., Mei, J., Liu, X., and Qi, H., 2018. Effect of triisopropanolamine on compressive strength and hydration of steaming-cured cement-fly ash paste. *Construction and Building Materials*. 192, 836–845